STACKING OF NAPPES WITH DIFFERENT PRESSURE-TEMPERATURE PATHS: AN EXAMPLE FROM THE MENDERES NAPPES OF WESTERN TURKEY

UWE RING[*], ARNE P. WILLNER[**], WOLF LACKMANN[*]

[*]*Institut für Geowissenschaften, Johannes Gutenberg-Universität, 55099 Mainz, Germany*

[**]*Institut für Geologie, Mineralogie und Geophysik, Ruhr-Universität, 44780 Bochum, Germany*

Abstract. Pressure-temperature (P-T) paths have been estimated from metapelitic rocks in the lowermost Çine nappe and the directly underlying Bozda© nappe of the Anatolide belt in western Turkey. Peak-metamorphic conditions in the lowermost Çine nappe are 670-730?C/?6.2-6.3 kbar. Prograde garnet (grt I) growth occurred largely before and during the formation of the regional S_{PA} foliation (the suffix 'PA' indicates a pre-Alpine age). Formation of a second garnet generation (grt II), which discordantly overgrew grt I, followed at 550-620?C/?6.4-6.5 kbar. Peak-metamorphic conditions in the underlying Bozda© nappe vary from 480-540?C/6.1-7.6 kbar at the base to 610-660?C/8.5-10.8 kbar at the top of the nappe and attest to an inverted metamorphic field gradient in the Bozda© nappe. Differential thermodynamic modelling (Gibbs method) yielded a prograde path for garnet growth during the formation of S_{PA}.

Because D_{PA} structures formed during prograde metamorphism, we relate them to crustal shortening, which was associated with a top-to-the-N/NE shear sense (in present-day coordinates). This event caused deformation of the Çine and Bozda© nappes under different metamorphic conditions. We propose, that the Çine nappe was heated by granitoid intrusions before being emplaced above a foreland unit. We speculate that the Bozda© nappe belonged to the lower parts of this foreland unit. Cross-cutting relationships of D_{PA} structures with dated granites indicates an age of ?540-550 Ma for this tectonometamorphic event. The final juxtaposition of the Çine nappe and Bozda© nappes, and also the inversion of the

metamorphic field gradient in the Bozda© nappe occurred during greenschist-facies conditions during the Alpine orogeny in the Eocene.

INTRODUCTION

A number of mountain belts on Earth result from superimposed orogenies. The reason why we treat this topic in our contribution to the *Festschrift* celebrating the 60th birthday of Alfred Kröner is that Alfred was facing this problem throughout his career, which took (and still takes) him to various Precambrian and Paleozoic orogens throughout the world, including orogens in southern Turkey. Alfred's main strategy to unravel aspects of superimposed orogenies is through extensive field work. He establishes crosscutting relationships of different granites and associated dikes in the field and then dates these rocks, using mainly U/Pb and Pb/Pb dating techniques on zircon. It is our belief that one of the cornerstones, which makes Alfred a distinguished and well-known geologist is the experience he gathered through almost 35 years of field work in numerous orogens on Earth. By dedicating this paper to Alfred, we would also like to stress that we still believe that detailed field work is the most important basis in geology.

In polyorogenic settings, it is usually difficult to unravel aspects of the tectonometamorphic history prior to the final orogeny. In the Anatolide belt of western Turkey, which is part of the Alpine Hellenide-Anatolide orogen in the eastern Mediterranean, synorogenic granite intrusions and their relationships to tectonometamorphic fabrics provide evidence for an orogeny at the Precambrian/Cambrian boundary (herein referred to as the Pan-African orogeny) and an Alpine orogeny in the Tertiary („engör and others, 1984; Kröner and „engör, 1990; Bozkurt and others, 1993; Hetzel and others, 1995a, 1998; Hetzel and Reischmann, 1996; Loos and Reischmann, 1999; Candan and others, 2000; Gessner and others, 2000a). Granitic intrusions dated at 230-240 Ma (Dannat, 1997; Koralay et al., 2000) are

thought to be related to an ill-defined Cimmerian event in the Triassic. Aspects of nappe tectonics prior to the Alpine orogeny are unkown.

Nappe emplacement will, in general, result in higher pressure-temperature (P-T) conditions in rocks of the lower plate (fig. 1A). However, one of the cornerstones during the discovery of the nappe concept in the Alps, the Ardennes and the Scottish Highlands (e.g. van der Linth, 1846; Lapworth, 1883; Bertrand, 1884; Termier, 1899; Lugeon, 1901) was the occurrence of rocks with higher-metamorphic grade above rocks with distinctly lower grade. Such a case appears to be common in orogens and is commonly used to diagnose nappe stacking. Nevertheless, the occurrence of high-grade on low-grade rocks demands that crustal shortening and nappe emplacement is associated with reduction of the overburden, i.e. exhumation, of the overriding nappe (fig. 1B). Assuming steady-state conditions, progressive stacking of nappes accompanied by exhumation will result in clockwise P-T paths, which are considered typical for Alpine-type mountain belts (England and Richardson, 1977; England and Thompson, 1984). Nonetheless, nappe emplacement may cause local anticlockwise P-T paths in nappes in a middle-plate position of a nappe package if the geotherm in the middle plate was higher than in the units above and below (fig. 1C). Kohn et al. (1992) reported such a case from the Appalachians of the eastern United States. Herein, we present another example of clockwise and supposedly anticlockwise P-T paths from the Menderes nappes of western Turkey.

In this article, we follow the “Kröner approach“ and use metamorphic and tectonic fabrics, and crosscutting relationships with granitic intrusions, which allow us to shed some light on metamorphism and nappe stacking during the Pan-African orogeny and re-stacking of these units and partial inversion of Pan-African metamorphism during the Alpine orogeny in western Turkey. We focus on the Bozda© nappe and the directly overlying Çine nappe of the lowest tectonometamorphic unit of the Anatolide belt and report aspects of the tectonometamorphic evolution of both nappes. The three issues we discuss are: (1) What is the relationship between Pan-African amphibolite-facies metamorphism, associated nappe stacking and emplacement of the eclogitic

lenses, which occur in both nappes (Candan

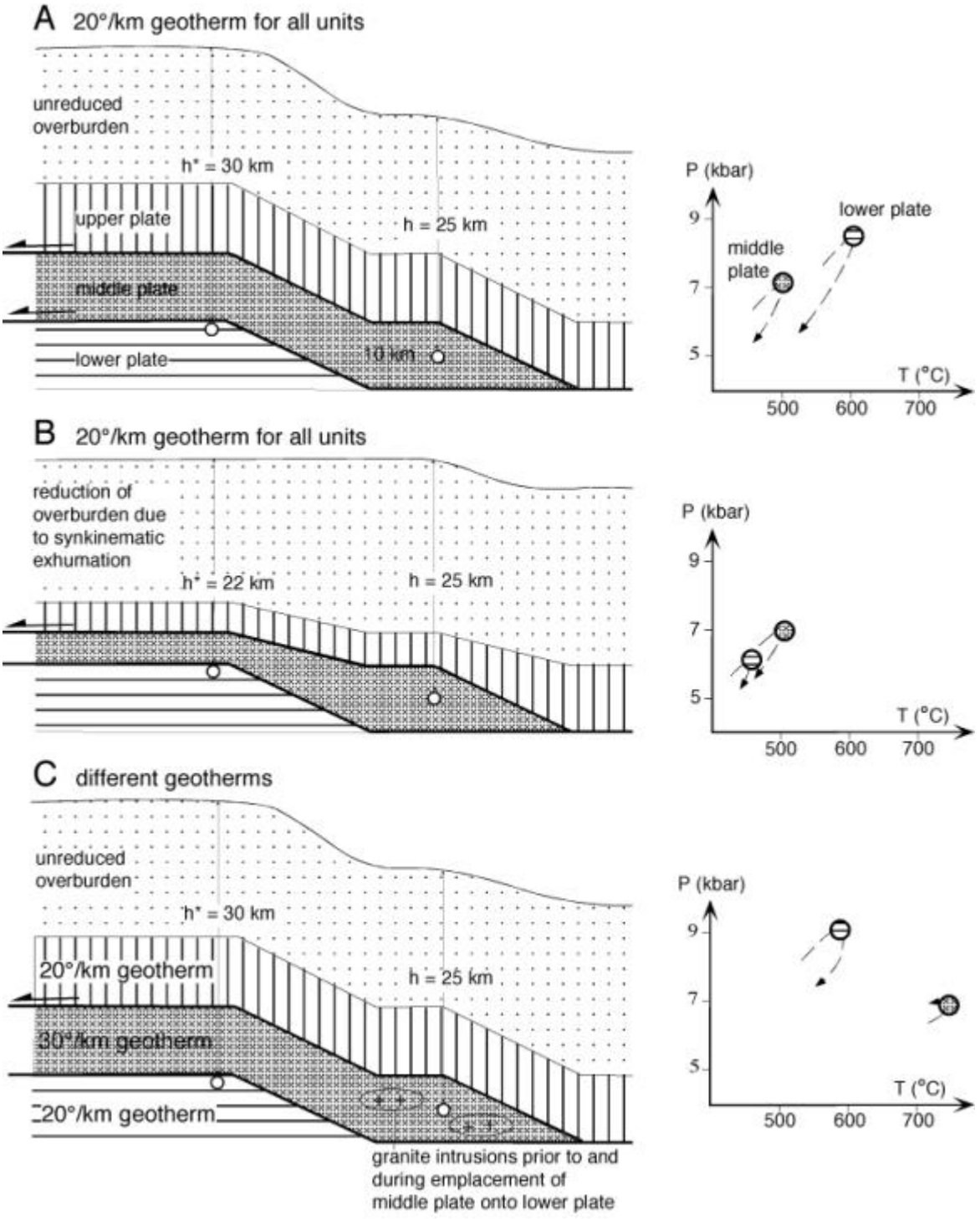

Fig. 1: Schematic nappe sequence and P-T paths for rocks in middle and lower plate; overburden thickness is converted into metamorphic pressure by assuming an average rock density of 2800 kg m^{-3}. (A) Emplacement of nappe without any accompanied exhumation resulting in highest P-T conditions for rocks in lower plate because h* is larger than h. (B) Nappe emplacement accompanied by exhumation. Higher-grade rocks will only be tectonically above lower-grade rocks if h* is smaller than h, which demands vertical thinning of the overriding nappe pile. Stacking and subsequent cooling by exhumation will cause clockwise P-T paths in examples (A) and (B). (C) Middle plate

characterized by a higher geotherm caused by heating due to intrusion of plutons. Emplacement of middle plate onto colder lower plate will cause cooling of middle-plate rocks and an anticlockwise P-T path; lower-plate rocks show increase in P-T conditions due to emplacement of hot middle plate and subsequent cooling. Such an example has been reported by Kohn and others (1992) and may relate to the example presented in this article.
et al., 2000)? (2) How do the different P-T paths in the Çine and Bozda© nappes relate to the mechanism of juxtaposition of both nappes? (3) What may have caused the inverted metamorphic field gradient in the Bozda© nappe?

SETTING

The Alpine Hellenide-Anatolide orogen in the eastern Mediterranean shows significant along-strike variations (fig. 2A and B). Large parts of the Hellenide belt have a granitic basement that yielded protolith ages of ?300-320 Ma (Reischmann, 1997; Engel and Reischmann, 1998; Ring and others, 1999a). Granitic basement rocks in the Menderes nappes of the Anatolide belt in western Turkey yielded ages of ?540-560 Ma and no Carboniferous granites have been found in the Menderes nappes so far (Hetzel and Reischmann, 1996; Dannat, 1997; Hetzel and others, 1998; Loos and Reischmann, 1999; Gessner and others, 2000a). Therefore, Ring and others (1999b) regarded the Menderes nappes as part of an exotic continental block in the Hellenide-Anatolide orogen. This continental block may have been part of Gondwana and apparently collided with the Angara craton of Siberia at the Precambrian/Cambrian boundary (Kröner and „engör, 1990).

The architecture of the Anatolide belt in western Turkey comprises three major tectonometamorphic units (table 1, figs. 2 and 3) which are characterized by different lithologies, protolith ages, pre-collisional paleogeography and orogenic history. This heterogeneous tectonic pile was assembled during Eocene crustal shortening, the D_{A3} event of Gessner and others (2000b) (the suffix ‘A’ indicates an Alpine age). Miocene

granitic rocks, which are related to crustal extension, intruded the northern part of the nappe pile.

The Lycian nappes and the Vardar-?zmir-Ankara suture zone represent the upper tectonometamorphic unit. The middle tectonometamorphic unit consists of the Dilek nappe and Selçuk melange. The deformation history of the middle unit includes two events (D_{A1} and D_{A2}) during Alpine high-pressure metamorphism followed by the emplacement of the middle unit onto the lower tectonometamorphic unit (the Menderes nappes) along the Cyclades-Menderes thrust (fig. 2C) during the greenschist-facies D_{A3} event. The emplacement of Alpine high-pressure units onto the Menderes nappes, which have no Alpine high-pressure overprint, indicates that D_{A3} thrusting was out of sequence (Ring et al., 1999b; Gessner et al., 2000b). The middle unit can be correlated with the Cycladic blueschist unit of the Hellenide belt in the Aegean (Candan and others, 1997; Ring and others 1999a and b; Gessner and others, 2000b; Okay, 2000). The middle and upper tectonometamorphic units were only affected by the Alpine orogeny.

The Menderes nappes

In this paper, we focus on the Menderes nappes, which form the lower tectonometamorphic unit of the Anatolide belt. The Menderes nappes comprise from top to bottom: (1) The Selimiye nappe, (2) the

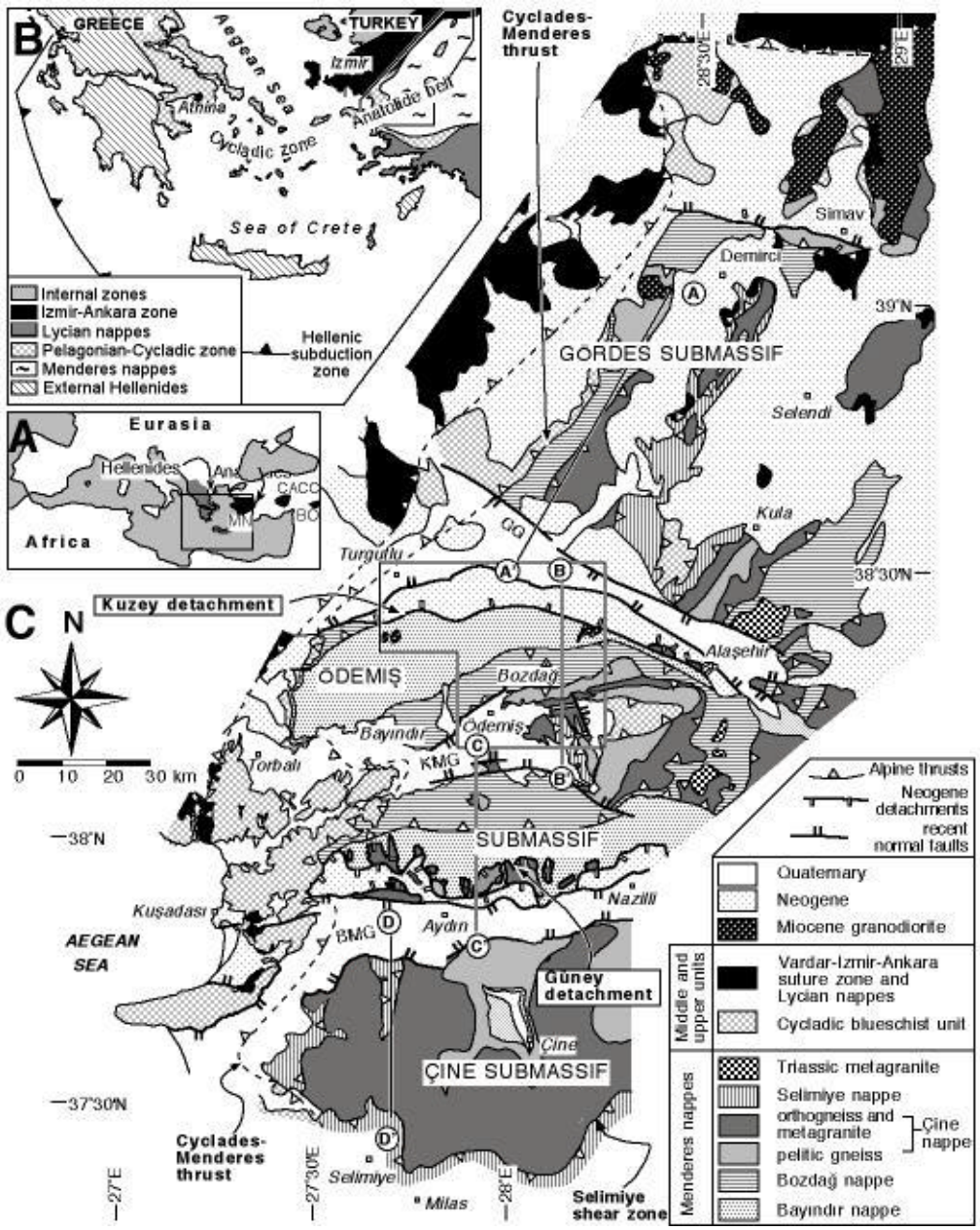

Fig. 2. (A) Generalized map of the Mediterranean showing Hellenides (grey) and Anatolides (black). The Anatolide belt in Turkey comprises the Menderes nappes (MN) in the west, the Central Anatolian crystalline complex (CACC) consisting of the Ni©de, Kir{ehir and Akda© massifs (Whitney and Dilek, 1998) in central Anatolia and the Bitlis orogen (BO) in the east. (B) Structure of the eastern Mediterranean. According Ring and others (1999a), we use the term 'Menderes nappes' for the deepest tectonometamorphic unit in the Anatolide belt in western Turkey, which is exotic with respect to any unit in the Aegean. (C) Simplified tectonic map of the Anatolide belt in western Turkey (this region is traditionally referred to as the Menderes Massif). The subdivison of the region into three submassifs (Gördes submassif, Ödemi{ submassif and Çine submassif) follows „engör (1987). Shown are the three major tectonometamorphic units; the subdivision of the Cycladic blueschist unit of western Turkey into the Dilek nappe and the Selçuk melange is shown in

the figure for clarity. Late-Alpine extension in the study area is expressed by two symmetrically arranged detachment-fault systems: the Kuzey detachment in the north and the Güney detachment in the south, both of which delimit the Central Menderes metamorphic core complex, which basically occupies the same area as the Ödemi{ submassif (fig. 3). Profile lines AA’, BB’, CC’ and DD’ for cross section in fig. 3 are indicated; box marks location of fig. 4; abbreviations: BMG = Büyük Menderes graben, KMG = Küçük Menderes graben, GG = Gediz graben.
Çine nappe, (3) the Bozda© nappe, and (4) the Bayindir nappe. With the exception of the Bayindir nappe, all nappes have a polyorogenic history (Gessner and others, 2000a).

The Selimiye nappe contains metapelite, metabasite and marble. In the lower part of the nappe, an undeformed metagranite intruded strongly deformed metapelite. The metagranite yielded a $^{206}Pb/^{207}Pb$ single-zircon age of 549 Ma (T. Reischmann, pers. comm. 1999), indicating a Precambrian protolith age for the surrounding metapelite. Fossil evidence indicates Devonian and Carboniferous protolith ages for some metasediments in the upper part of the Selimiye nappe (Schuiling, 1962; Ça©layan and others, 1980).

Most of the Çine nappe consists of deformed orthogneiss and largely undeformed metagranite. Pelitic gneiss, which in part shows migmatitic fabrics (Hetzel, 1995), eclogite and amphibolite also crop out. The pelitic gneiss north of Birgi (fig. 4) is in part made up of alternating sequences of pelitic and quartz-rich (psammitic) layers and resembles a former turbiditic sequence. Most orthogneiss intruded at ?540-560 Ma (Hetzel and Reischmann, 1996; Dannat, 1997; Loos and Reischmann, 1999) and the ages appear to young northward. Very few scattered metagranites have protolith ages of ?530-540 Ma (Dannat, 1997; Loos and Reischmann, 1999; T. Reischmann, pers. comm., 2000). The Birgi metagranite (fig. 4) intruded pelitic gneiss of the lowermost Çine nappe and yielded a U/Pb zircon age of 551?1.4 Ma, which has been interpreted as a crystallization age (Hetzel and others, 1998). In the vicinity of the Birgi metagranite, abundant granitic dikes and pegmatites oriented parallel to the penetrative foliation, occur in the pelitic gneiss. $^{206}Pb/^{207}Pb$ single-zircon dating of migmatites from the Ödemi{ and Gördes submassifs generally

yielded ages of ?540-550 Ma for migmatization (Dannat and Reischmann, 1999; T. Reischmann, pers. comm., 1999).

The underlying Bozda© nappe is made up of metapelite with intercalated amphibolite, eclogite and marble lenses. Protolith ages of all rock types are unknown, but geologic constraints (Gessner and others, 2000a) suggest a Precambrian age for at least parts of these rocks. The Bozda© nappe was intruded by granitoids at 230-240 Ma (Dannat, 1997; Koralay and others, 2000).

The Bayindir nappe contains phyllite, quartzite, marble and greenschist of inferred Permo-Carboniferous and Mesozoic age (O. Candan, pers. comm., 1999; Okay, 2000), but Early Tertiary depositional ages for parts of the nappe are likely. The rocks were affected by a single Alpine greenschist-facies metamorphism at ?37 Ma (Lips, 1998) during the D_{A3} event.

The Çine and Bozda© nappes are characterized by systematically oriented ductile structures. The D_{PA} event (sensu Gessner and others, 2000a; the suffix ‘PA’ indicates a pre-Alpine age) caused top-to-the-N/NE shear (in present-day coordinates) during amphibolite-facies metamorphism in both nappes. Oberhänsli and others (1997) and Candan and others (2000) reported that amphibolite-facies metamorphism overprinted earlier eclogite-facies relics in some lenses in the Çine and Bozda© nappes. Candan and others (2000) distinguished between eclogite, which equilibrated at 580-660?C and a

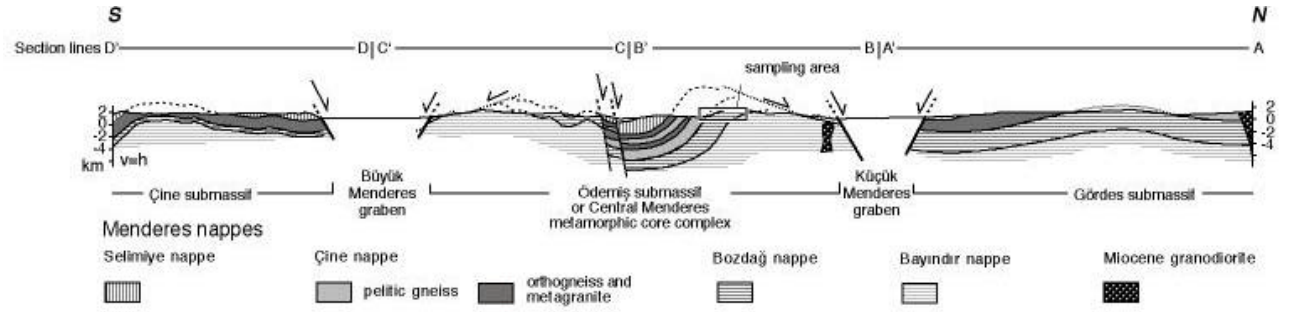

Fig. 3. Schematic north-south cross section showing architecture of nappe package, which was assembled during Alpine (D_{A3}) top-to-the-S out-of-sequence nappe stacking (for profile lines and symbols of thrusts, detachments and faults refer to fig. 2). The sampling area (box) is situated in a unique area where a complete crustal section is tilted and therefore exposed at the flank of a huge syncline. This syncline is due to large-scale folding during the late phase of bivergent detachment faulting, which delimits Central Menderes metamorphic core complex (Gessner, 2000). For geometric viability section planes are oriented parallel to mean orientation of L_{A3}; trace of foliation is projected into section plane and used to infer the geometry of sub-surface structures.

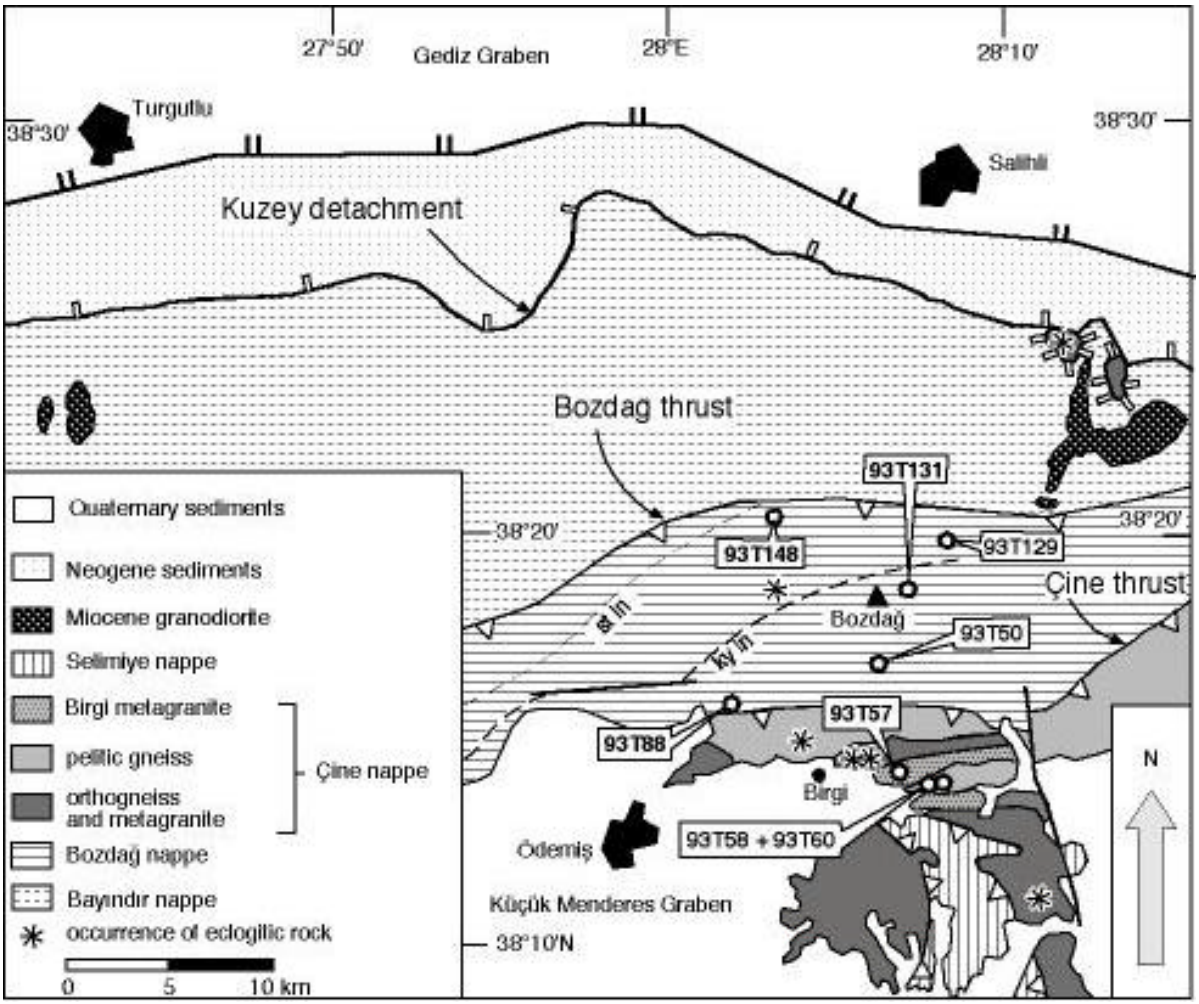

Fig. 4. Tectonic map of northern Ödemi{ submassif showing st-in and ky-in isograde (Ashworth and Evirgen (1985) and this study). Isograde and also our thermobarometric calculations show

increasing P-T conditions in the Bozda© nappe from north to south, i.e. structurally upward. Also shown are sample localities (refer to fig. 2 for location of map); eclogite occurrences (Oberhänsli and others, 1997; Candan and others, 2000); thrusts and normal faults as in fig. 2.

minimum pressure of ?15 kbar and eclogitic gabbro, which equilibrated at 510-690?C and minimum pressures of 10-12 kbar. In the Çine nappe, both eclogitic rock types occur, whereas in the Bozda© nappe, only eclogitic gabbro have been reported so far (Candan and others, 2000). The D_{PA} structures deformed the eclogite during retrogression and reflect the first regionally mapable deformation event that affected the eclogite and the enveloping rocks of the Çine and Bozda© nappes together. In the Çine nappe, D_{PA} affected orthogneiss dated at ?550-560 Ma and a crosscutting metagranite from the southern Çine nappe yielded a $^{206}Pb/^{207}Pb$ zircon age of 547?1.0 Ma (Gessner and others, 2000a). As we will show below, the metamorphic evolution of the metapelite from the Çine and Bozda© nappes is different from the metamorphic evolution of the intercalated eclogitic rocks. Therefore, we regard the Çine and Bozda© nappes to be composite nappes.

Preliminary structural work in the Selimiye nappe suggests that an early deformation event occurred during lower-amphibolite-facies conditions. From our scarce data, it appears feasible that this event occurred before the intrusion of the 549-Ma metagranite and corresponds with the top-to-the-N/NE shear in the Çine and Bozda© nappes. Structures belonging to this event were overprinted by the Alpine D_{A3} top-to-the-S Selimiye shear zone (also termed South Çine shear zone; Lips, 1998), which separates the Selimiye nappe from the underlying Çine nappe. Hetzel and Reischmann (1996) reported static growth of garnet at temperatures >450?C after D_{A3} in the Selimiye shear zone and showed that $^{39}Ar/^{40}Ar$ muscovite ages of 43-37 Ma constrain slow cooling after the post-D_{A3} garnet-growth event.

In the Selimiye, Çine and Bozda© nappes, D_{PA} fabrics were overprinted by Alpine greenschist-facies D_{A3} structures, which

are largely localized at the nappe contacts (Gessner et al., 2000b). The Eocene D_{A3} event produced a variably spaced mylonitic shear-band foliation and a stretching lineation associated with top-to-the-S kinematic indicators at the contacts separating the Selimiye, Çine, Bozda© and Bayindir nappes from each other. D_{A3} structures affected the interiors of these nappes heterogeneously; in the Çine and Bozda© nappes they are pervasive only in a few zones within the nappes. During and after D_{A3}, chlorite and white mica, in part also biotite and garnet (see above) were stable. Very generalized, this suggests temperatures of ?400->450?C and pressures of ?4-6 kbar during D_{A3}. Contractional D_{A3} structures were overprinted in the northern Ödemi{ submassif by ductile D_{A4} shear bands. These shear bands developed simultaneously with the intrusion of the Miocene granodiorites during NNE-oriented horizontal extension (Hetzel and others, 1995a; Isik and Tekeli, 2000; Gessner and others, 2000b). A later phase of bivergent brittle detachment faulting commenced in Late Miocene time and is associated with the development of the still active Menderes graben („engör, 1987; Hetzel and others, 1995b; Gessner and others, 2000c).

The Alpine amalgamation of the Anatolide belt resulted in a complicated nappe structure (Ring et al., 1999b; Gessner et al., 2000b), but aspects of the Pan-African tectonic evolution of the belt are poorly known. Candan and Dora (1997) and Candan et al. (2000) distinguished a tectonometamorphically homogeneous Pan-African basement (or core series) from younger sequences, the so-called cover series. The core series of Candan and Dora (1997) and Candan et al. (2000) largely compare to the Çine and Bozda© nappes, whereas the cover series compare to the middle tectonometamorphic unit and the Bayindir and Selimiye nappes of Ring et al. (1999b), Gessner et al. (2000b) (fig. 2). The general architecture depicted in the cross section (fig. 4) and the very different metamorphic evolution of the middle tectonometamorphic unit, the Bayindir nappe and the Selimiye nappe make it hard for

us to envision that they all belong to a single, coherent Alpine tectonic unit.

In summary, the data suggest that the D_{PA} event occurred at ?540-550 Ma under amphibolite-facies conditions. Local migmatization apparently coincided with granitoid emplacement, which occurred mainly prior to and during, but also after D_{PA}. The present architecture of the Anatolide belt in western Turkey was caused by the Eocene D_{A3} event.

ANALYTICAL PROCEDURES

The mineral analyses were obtained with a Cameca SX 50 microprobe at Ruhr-Universität Bochum, Germany, and a Jeol Superprobe (JXA 8900RL) at Johannes Gutenberg-Universität Mainz, Germany. Operating conditions were an acceleration voltage of 15 kV, a beam current of 15 nA, 20 s counting time per element. For feldspar and mica analyses a slightly defocussed beam of 8 ?m was used in order to avoid loss of alkalies. Standards used were the following [those for Mainz are given in brackets]: synthetic pyrope [wollastonite] for Si, synthetic pyrope [corundum] for Al, rutile [pyrophanite] for Ti, glass of andradite composition [hematite] for Fe, synthetic pyrope [MgO] for Mg, glass of andradite composition [wollastonite] for Ca, jadeite [albite] for Na, K-bearing glass [orthoclase] for K, NaCl [tugtupite] for Cl, topaz [F-phlogopite] for F, Cr_2O_3 for Cr, Ba-silicate glass [barite] for Ba (L?). The PAP (Bochum) and a ZAF (Mainz) procedure was used for matrix correction. The mineral analyses are considered to be accurate within a range of ?3% (relative) on any given grain. Element distribution maps for four elements were simultaneously produced by stepwise scanning over rectangular areas using the Jeol Superprobe in Mainz.

The following abbreviations are used in the text, tables and figures: Adr = andradite, Alm = almandine, An = anorthite, And = andalusite, As = aluminosilicate, Bt = biotite, Chl = chlorite, Cld = chloritoid, Grt = garnet, Grs = grossular, Ky = kyanite, Kfs = potassium feldspar, Ms = muscovite, Phl = phlogopite, Pl =

plagioclase, Prp = pyrope, Qtz = quartz, Sil = sillimanite, Sps = spessartine, St = staurolite.

For geothermobarometry, we calculated multivariant reactions using the Ge0calc software (Brown and others, 1989) with the internally consistent data set of Berman (1988) with the activity models of following solid solutions: garnet (Berman, 1990), biotite (McMullin and others, 1992), plagioclase (Fuhrman and Lindsley, 1988) and white mica (Chatterjee and Froese, 1975). For the assemblage garnet-biotite-plagioclase-muscovite-paragonite-staurolite-quartz-H_2O we modelled P-T paths in the system MnO-Na_2O-CaO-K_2O-FeO-MgO-Al_2O_3-SiO_2-H_2O (MnNCKFMASH) using the software "Gibbs ‘90" (version 7) (Spear and others, 1991) with a modified data set of Reinecke (1998). The calculated P-T data are listed in table 2; mineral analyses of garnet, biotite, white mica, plagioclase and staurolite are listed in tables 3-7. We consider the P-T data to be accurate within a range of ?1 kbar and ?50?C. A full set of analyses may be obtained from the second author.

MESOSCOPIC STRUCTURES, PETROGRAPHY AND MINERAL CHEMISTRY

Five metapelite samples from the Bozda© nappe, two samples of pelitic gneiss from the lowermost Çine nappe (fig. 5A) and one sample from the Birgi metagranite (fig. 5B) were selected for petrologic work. The metapelitic rocks from both nappes are characterized by a penetrative foliation and associated N/NE-trending stretching lineation. These structures can be ascribed to the D_{PA} event of Gessner and others (2000a). In the sampling area, greenschist-facies D_{A3} structures are prominent in the immediate vicinity of the Çine and Bozda© thrusts (fig. 4), but also occur in a few zones within the Çine and Bozda© nappes (fig. 5C-F). The D_{A3} structures were overgrown by locally abundant albite porphyroblasts in greenschist and metapelite, which are extensive at the Bozda© thrust. In the vicinity of this nappe contact, D_{A4} extensional shear bands occur and become more penetrative to the north of the Bozda© thrust. The D_{A4} shear bands

deform the albite porphyroblasts (Hetzel, 1995; Hetzel et al., 1998; Gessner and others, 2000b).

Çine nappe

Pelitic gneiss.–The general mineral assemblage is garnet-biotite-white mica-plagioclase-quartz-sillimanite. Garnet is up to 5 mm in size and shows two distinct generations. Garnet I is idioblastic and contains tiny inclusions of quartz and fibrolitic sillimanite, particularly in the core. In the rims of garnet I, large biotite, white mica, quartz, rutile and ilmenite inclusions occur. Some inclusions are oriented parallel to an oblique internal foliation. Garnet I grew largely pre- but also synkinematically with respect to S_{PA} and biotite, white mica and quartz grew in strain shadows around grt I (fig. 5A). The asymmetry of the strain shadows is consistent with top-to-the-N/NE shear. Garnet I was overgrown by a second, more skeletal garnet (grt II), which is intergrown with biotite. Garnet II mainly grew at the expense of biotite and has also inclusions of quartz, white mica, ilmenite and rutile. Garnet II overgrew biotite in pressure shadows around grt I and also matrix biotite oriented parallel to S_{PA} (fig. 5A). Garnet II did not only nucleate on grt I but also grew as xenoblastic grains of rather variable size particularly within biotite aggregates. Fabric relationships indicate late- to postkinematic growth of grt II with respect to S_{PA}.

Garnet I is associated with red-brown biotite, the latter of which grew mimetically with respect to S_{PA}, i.e. is oriented parallel to S_{PA} and also crosscutting it. Fibrolite grew aligned along rims of oriented biotite. Quartz films formed at the contact between biotite and fibrolite. White mica is rare and mostly

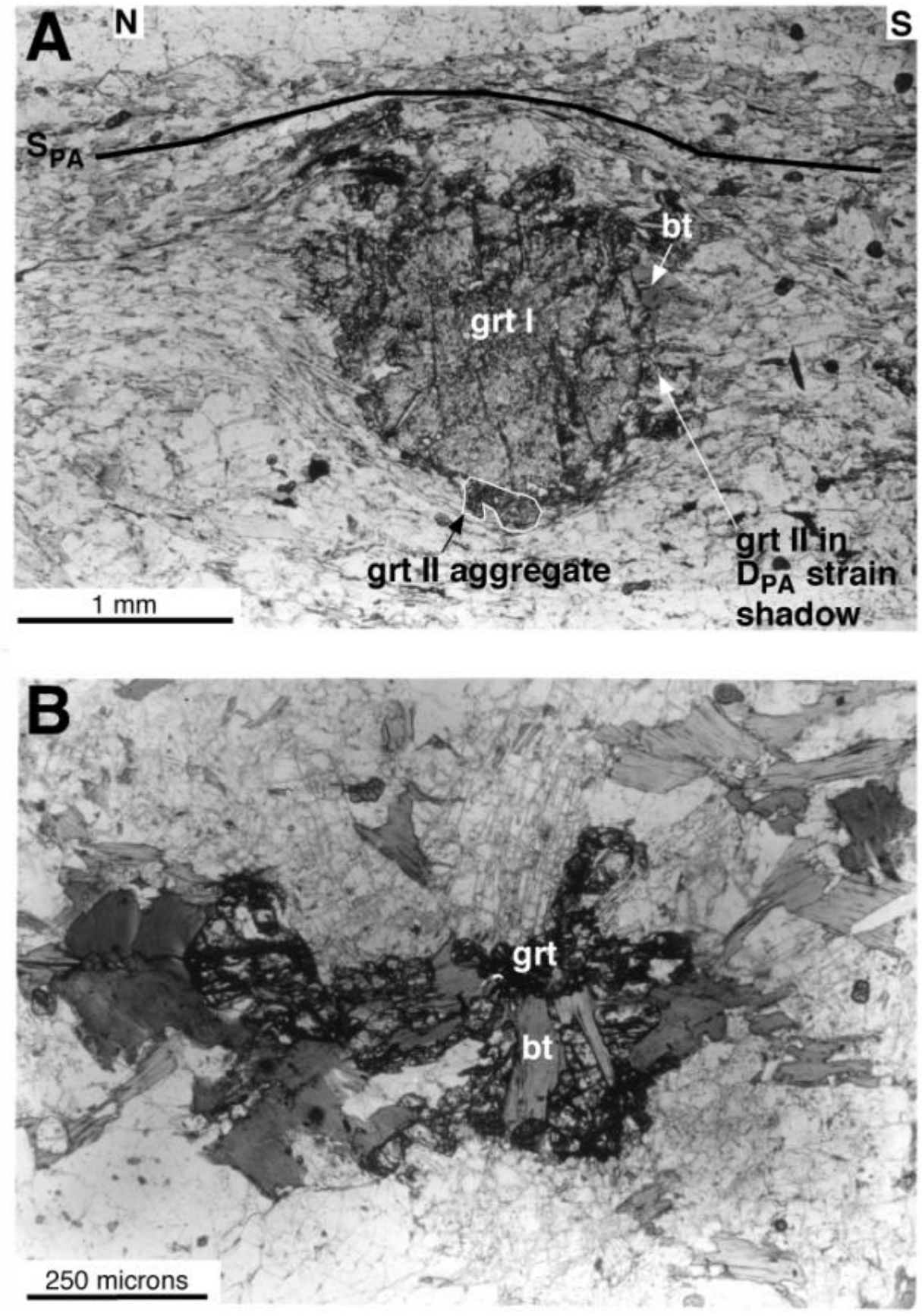
A
N
S
S_{PA}
bt
grt I
grt II aggregate
grt II in D_{PA} strain shadow
1 mm
B
grt
bt
250 microns

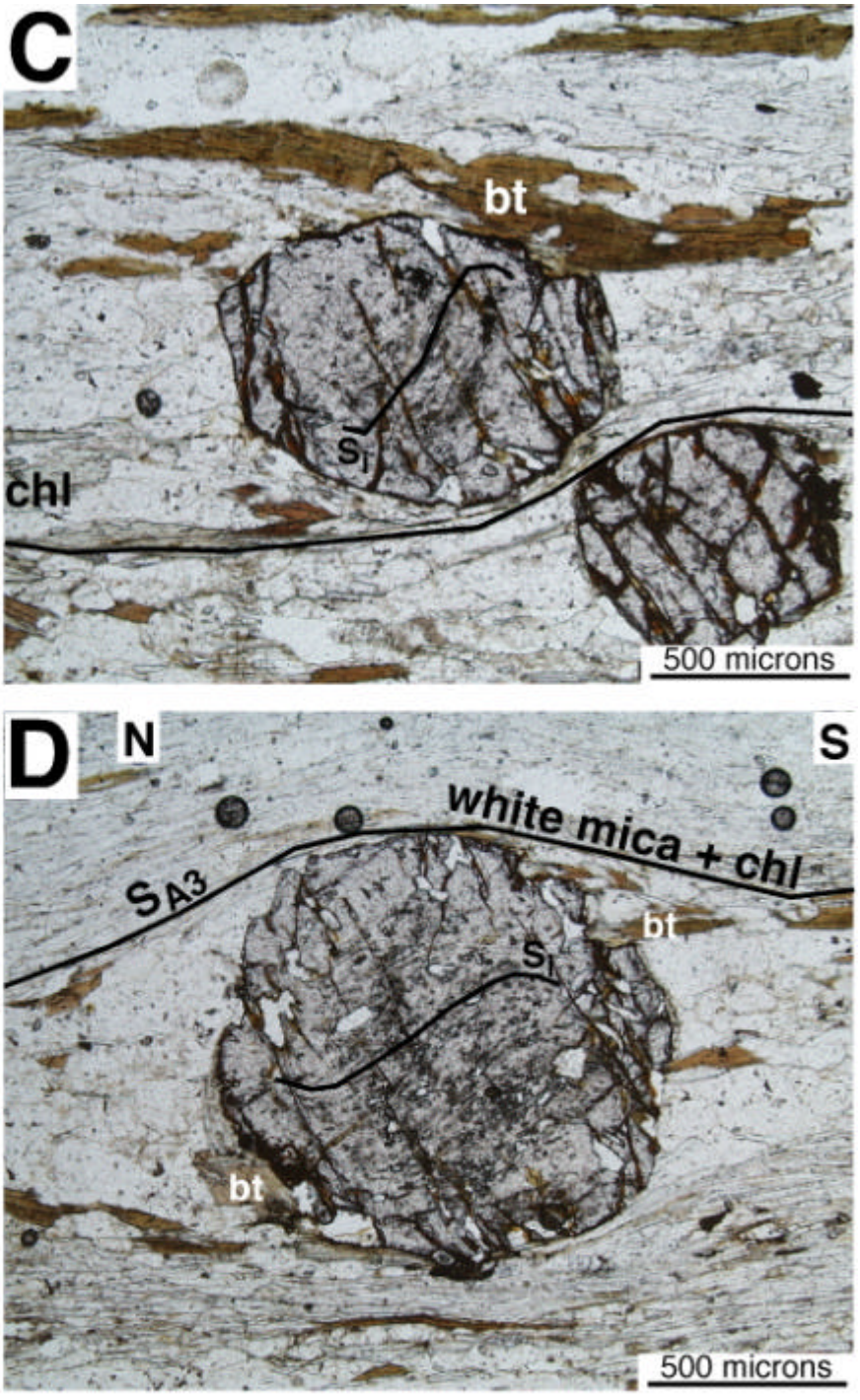
C
bt
S_I
chl
500 microns
D
N
S
white mica + chl
S_{A3}
bt
S_I
bt
500 microns

Fig. 5. Photomicrographs, all plane-polarized light: (A) Subidioblastic grt I overgrown by xenoblastic grt II in Çine nappe; inclusions in garnet have no obvious preferred orientation; asymmetry of strain shadows around grt I indicate top-to-the-N/NE sense of shear associated with development of S_{PA}; grt II overgrew oriented mica in strain shadows. Sample 93T60. (B) Garnet growing at grain boundaries of biotite in Birgi metagranite. Sample 93T57. (C) Garnet core with sigmoidal internal foliation (S_i) and postkinematic rim lacking internal fabric. Sample 260 from Bozda© nappe. (D) Garnet core with slightly curved S_i; garnet rim has no internal foliation; S_{A3} foliation around garnet is made up of chlorite, white mica and quartz; biotite in strain shadows and in foliation planes breaks down to chlorite. Sample 260 from Bozda© nappe. (E) Garnet core with slightly curved S_i and rim without internal fabric; large biotite in asymmetric strain shadow grew at expense of grt rim and incipiently breaks down synkinematically with respect to S_{A3} to chlorite. Sample 260 from Bozda© nappe. (F) Garnet with core rich in graphite inclusions; postkinematic grt rim is partly transformed to chlorite; chlorite, white mica and quartz make up external S_{A3}, which wraps around grt; biotite in matrix is chloritized along D_{A3} shear band. Sample 260 from Bozda© nappe. Sample 260 is described in detail in Gessner (2000).

Fig. 6. Element distribution maps for Mg, Ca, Fe and Mn. (A) Garnet I from sample 93T60 of Çine nappe; note small grt II with higher Ca and lower Mn contents around grt I. (B) Garnet from sample 93T131 of Bozda© nappe. We distinguish a core, which is in general synkinematic and characterized for instance by low Mg contents, a postkinematic rim characterized by relatively high Mg and low Ca contents and an outermost very thin rim characterized by increasing Mn and decreasing Mg, Ca and Fe contents.

aligned parallel to biotite but did not break down in the presence of quartz. S_{PA}-parallel quartz-feldspar aggregates are widespread; these aggregates also express a strong N/NE-trending stretching lineation on S_{PA}. Rutile and ilmenite are common oxide phases in the matrix; ilmenite overgrew rutile.

The two texturally distinct garnet generations can also be distinguished chemically (table 3). Garnet I shows a weak growth zonation as indicated by a faint bell-shaped zonation of Mn (X_{Sps}=0.12-0.02 from core to rim). Ca (X_{Grs}=0.06-0.02) also decreases. In contrast, Mg (X_{Prp}=0.15-0.28), Fe (X_{Alm}=0.64-0.76) and X_{Mg} (0.16-0.33) slightly increase towards the idioblastic rim (fig. 6A).

Overgrowth of skeletal grt II is strongly discontinuous with a marked decrease of Mn, Fe, Mg and X_{Mg} and an increase of Ca at the contact between rims of grt I and grt II. Garnet II is also characterized by distinct zoning patterns. The Ca content (X_{Grs}=0.04-0.13) is patchy, but tends to increase towards the rim. In contrast, Fe (X_{Alm}=0.74-0.61), Mn (X_{Sps}=0.03-0.01), Mg (X_{Prp}=0.25-0.17) and X_{Mg} (0.22-0.14) decrease irregularly towards the rim.

In all analyzed samples, biotite has a narrow range of variation in X_{Mg} (0.54-0.67) and Ti (0.13-0.19 per formula unit, pfu for short), but variable contents of Si (2.69-2.82 pfu) and Al^{VI} (0.30-0.45 pfu) (table 4). There is no clear correlation between these parameters; however, biotite intergrown with grt II has the highest X_{Mg}. The composition of white mica is characterized by low Si contents (3.15-3.24 pfu) and a low paragonite component (4-14 mol%) (table 5). White-mica inclusions in grt I have similar Si values, but generally lower Na contents than matrix white mica. Plagioclase is invariably oligoclase (15-26 mol% anorthite). Plagioclase inclusions in grt I have a low anorthite content (table 6).

Birgi metagranite.–The metagranite primarily consists of potassium feldspar, plagioclase, biotite, white mica and quartz

(Hetzel, 1995). A tectonic foliation is visible at the margins of the granite; magmatic fabrics are still preserved in its interior. Evidence for a pre-foliation metamorphic overprint of the granite is the growth of garnet at the expense of biotite, particularly along grain boundaries of large biotite grains (fig. 5B) (Hetzel, 1995; Hetzel et al., 1998). Some garnet also grew within biotite. White mica and sillimanite formed at the margins of biotite, and fibrolite occurs at feldspar grain boundaries (Hetzel, 1995). Sericitization of plagioclase is common.

Garnet does not show any systematic zonation. Compositional variation is Grs_{5-11}-Alm_{68-76}-Prp_{10-16}-Sps_{5-10}. X_{Mg} in biotite varies from 0.40 to 0.53, the Ti content of 0.08-0.22 pfu is high and the Si content is on the order of 2.58-2.74 pfu. White mica is characterized by low Si contents of 3.08-3.22 pfu, and a low paragonite component (4-6 mol %). Plagioclase contains 17-25 mol% anorthite.

Bozda© nappe

The mineral assemblage in metapelite of the Bozda© nappe is garnet-biotite-white mica-quartz-plagioclase-staurolite-(kyanite)-(chlorite). Ashworth and Evirgen (1985) reported an increasing

metamorphic grade from the base to the top of the Bozda© nappe as indicated by the staurolite-in and kyanite-in isograds (fig. 4).

Garnet grain size ranges between 0.3 and 0.8 mm. Garnet has cores containing tiny inclusions of quartz and graphite oriented parallel to a relic internal foliation, which is oblique to the external penetrative S_{PA} foliation. Sigmoidal inclusion trails of quartz and graphite indicate synkinematic garnet growth (Hetzel, 1995) with respect to S_{PA} (fig. 5C-E). In samples, which do not show pronounced Alpine deformation, quartz, biotite and white mica grew in associated asymmetric strain shadows and indicate top-to-the-N/NE shear. In (hyp)idioblastic garnet rims, very few, but large inclusions of quartz, biotite, rutile, ilmenite and white mica occur. The rims show no internal fabric and grew post S_{PA}, but pre S_{A3} (fig. 5C-F).

Biotite and white mica grew mimetically with respect to the S_{PA} foliation. Both micas contain ilmenite inclusions. Plagioclase occurs in two distinct generations; one with recrystallized quartz in bands parallel to S_{PA} (pl I), and a second plagioclase (pl II) occurring as large porphyroclasts, which contain oriented white mica and quartz inclusion trails. Ashworth and Evirgen (1985) described two coexisting plagioclase generations defining the peristerite miscibility gap.

Staurolite also grew parallel to S_{PA}, is generally xenoblastic and contains abundant inclusions of quartz and occasionally white mica. Similarly skeletal kyanite is oriented parallel to S_{PA} and contains quartz, rutile and ilmenite as inclusions. Kyanite crystals also cut across S_{PA}. Rutile and ilmenite are also present in the matrix. Ilmenite generally overgrew rutile and is oriented parallel to S_{PA}. Tourmaline is another common accessory phase.

The pattern of garnet zoning is remarkably similar in all five analyzed samples (table 3). A core, a rim and a tiny outermost rim can be distinguished chemically (fig. 6B). Ca is not zoned in the core, but decreases strongly towards the rim (X_{Grs}=0.08-0.27). Fe (X_{Alm}=0.42-0.77) and Mg (X_{Prp}=0.03-0.15) increase towards the

rim, as does X_{Mg} (0.05-0.17). Mn depicts a bell-shaped profile, but increases notably again at the outermost rim (X_{Sps}=0.01-0.22). Ti decreases from core to rim (0.03-0.002 pfu).

Biotite shows variations among samples in X_{Mg} (0.42-0.56), Si (2.61-3.00 pfu), Al^{VI} (0.37-0.54 pfu) and a high Ti content (0.17-0.28 pfu) (table 4). White mica is muscovite (3.0-3.2 Si pfu) with a notable paragonite component (X_{Na}=0.05-0.30) (table 5). In three samples (93T88, 93T129, 93T148), an additional coexisting paragonite (X_{Na}=0.83-0.92) occurs and the X_{Na} in the corresponding muscovite is 0.21-0.30. Plagioclase I between S_{PA} planes has 12-26 mol% anorthite component with irregular zoning patterns, but the general trend shows increasing Ca content from core to rim. In contrast, the large intertectonic porphyroclasts (pl II) are albite (1-2 mol% anorthite) (table 6). Staurolite has Fe-rich compositions (X_{Fe}=0.78-0.82) with low Mn (0.019-0.27 pfu) and moderate Ti contents (0.040-0.092 pfu) (table 7).

Post-S_{PA} mineral growth includes chlorite, white mica and in part biotite recrystallization parallel to S_{A3}. In zones of strong D_{A3}, S_{PA} planes are completely transposed into S_{A3} as characterized by breakdown of garnet to biotite and mainly chlorite (fig. 5E and F). Biotite/chlorite replacement of garnet becomes more frequent towards the upper and lower nappe contacts of the Bozda© nappe, where chlorite is stable in D_{A3} shear bands. Retrogression of garnet to chlorite resulted in irregular garnet rims; some garnet grains are entirely replaced by chlorite. A further retrograde phase is abundant sericite at grain boundaries or fissures in kyanite, garnet, staurolite and biotite. Ilmenite also grew parallel to S_{A3}.

A ubiquitous feature in samples 93T129 and 93T148 from the lowermost (northern) part of the Bozda© nappe is the intertectonic growth of abundant albite (pl II) porphyroclasts between D_{A3} and D_{A4}. These albite porphyroclasts also occur across the Bozda© thrust in the upper Bayindir nappe and commonly overgrew and thus obscured D_{A3} structures. In the northern Ödemi{ submassif, the albite porphyroclasts were dragged into discrete

D_{A4} shear bands, in which new chlorite grew and quartz partly recrystallised. Plagioclase II porphyroclasts rotated between discrete D_{A4} shear bands. In these shear bands, chlorite grew at the expense of garnet, staurolite and biotite, partly together with white mica.

GENERAL PHASE RELATIONSHIPS AND GEOTHERMOBAROMETRY

Çine nappe

Pelitic gneiss.–The mineral assemblage, the fibrolitic sillimanite, white mica inclusions in both garnet generations and the occurrence of leucosomes of granitic composition (Hetzel, 1995) is interpreted to show that both garnet generations grew within the reaction field of the following continuous reaction, which is limited by the staurolite+muscovite+quartz and muscovite+quartz breakdown curves (fig. 7):

$$\text{Muscovite}_{\text{white mica}} + \text{(Fe,Mg) garnet}_{\text{grt}} = \text{(Fe,Mg) biotite}_{\text{bt}} + \text{sillimanite} + \text{quartz} \quad (1)$$

Maximum temperatures were close to the wet granite solidus. Further garnet-forming reactions for grt I and II are:

$$\text{grossular}_{\text{grt}} = 3\ \text{anorthite}_{\text{pl}} + 2\ \text{aluminosilicate} + \text{quartz} \quad (2)$$

$$\text{(Fe,Mg) garnet}_{\text{grt}} + \text{muscovite}_{\text{white mica}} + \text{grossular}_{\text{grt}} = \text{(Fe,Mg) biotite}_{\text{bt}} + 3\ \text{anorthite}_{\text{pl}} \quad (3)$$

The preservation of a weak growth zonation of Mn, Mg and Fe in grt I might indicate that diffusion effects were minor and hence residence time at high temperature may have been relatively short. The widespread formation of fibrolite at the contact with biotite coated by tiny films of quartz is interpreted as an effect of a cation-solution reaction such as:

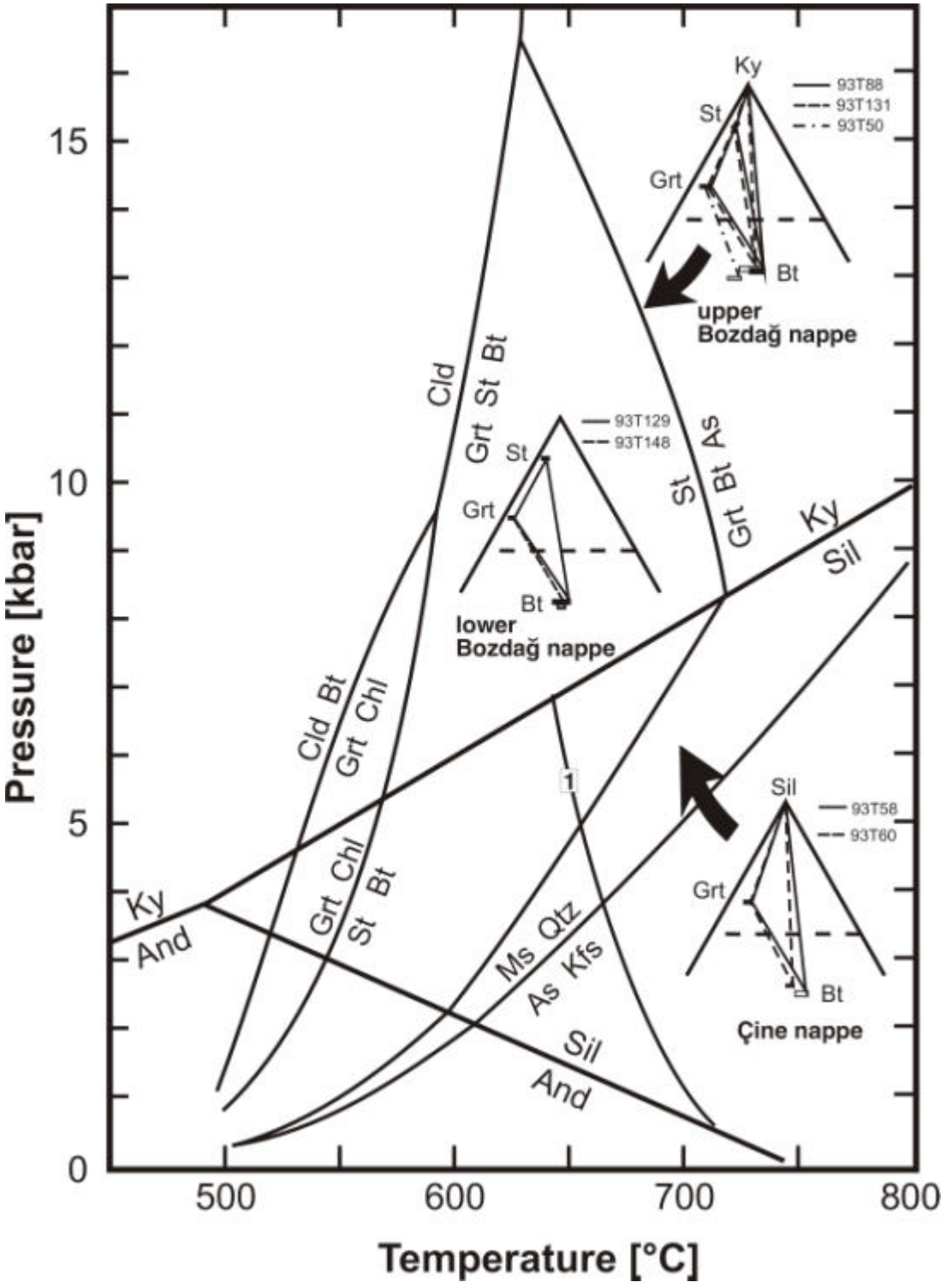

Fig. 7. Assemblages for samples 93T129 and 93T148 (lower Bozda© nappe), samples 93T131, 93T88 and 93T50 (middle and upper Bozda© nappe) and samples 93T58 and 93T60 (lower Çine nappe) in AFM diagrams projected from quartz, white mica and vapor in relation to KFMASH petrogenetic net (Spear and Cheney, 1989). Reactions shown also involve quartz, white mica and vapor; aluminosilicate stability fields (Holdaway, 1971); wet granite solidus (1) (Johannes, 1985).

2 biotite + 14 H^+ = 1 sillimanite + 2 K^+ + 6 Fe^{2+} + 5 quartz + 9 H_2O. (4)

This reaction proceeds with increasing pressure and temperature (Willner, 1992, 1995). Growth zoning in grt I, particularly increasing X_{Mg}, is compatible with increasing temperature and pressure within the field of reaction (1). In figure 8, isopleths of biotite and garnet compositions were constructed from intersection of the Mg- and Fe-end-member curves of reaction (1) calculated for the approximate compositional variation in an average Çine metapelite reduced to the pure KCFMASH system. A relatively flat prograde P-T path for growth of grt I within the stability field of sillimanite results if the composition of the coexisting biotite would also constantly shift to more Fe-rich compositions.

For evaluating P-T conditions during growth of grt I, rim compositions of grt I were combined with lowest X_{Mg} biotite and the composition of white mica enclosed in grt I. Reasonable intersection of reactions (1)-(3) and the Fe-Mg exchange reaction between biotite and garnet occurs only when plagioclase with the lowest An content within grt I is used for the calculation of the coexisting assemblage. Conditions of 670-730?C/6.2-6.3 kbar are indicated, which are compatible with the petrogenetic net (fig. 7). These P-T conditions partly extend beyond the granite minimum-melting curve, which is compatible with field evidence for migmatization.

Growth of the discontinuously overgrowing grt II may be interpreted as follows. Notable increase of Ca in grt II at its contact with grt I might either be due to an increase in pressure in the presence of plagioclase (continuous reactions (2) and (3)) or, if the relatively flat slopes of the continuous Ca-garnet producing reactions (2) and (3) are considered, a near-isobaric temperature decrease. The generally observed intergrowth of grt II with the highest X_{Mg} biotite indicates growth at lower temperature. Because similar inclusion assemblages are observed

in both garnets, there is no indication for a change in the limiting mineral assemblage as a cause for the discordant overgrowth of grt II. A pronounced change of the direction of the P-T path such as isobaric cooling can be an explanation. Growth zoning in grt I is preserved and skeletal growth of grt II may indicate rapid growth during cooling. An alternative could be growth of grt II during pressure increase after renewed nappe stacking following cooling to intermediate temperatures. Nonetheless, decreasing X_{Mg} towards the rim in the given assemblage is compatible with cooling and some pressure release after maximum P-T conditions were reached during growth of grt I. Formation of grt II led to local equilibrium at contacts with plagioclase with higher An contents at the rims.

Biotite, plagioclase and white mica in contact with grt II result in good intersection of the multivariant reactions (1)-(3) and the Fe-Mg exchange reaction of biotite and garnet and characterize the P-T conditions during growth of grt II at 550-620?C/6.4-6.5 kbar. These P-T conditions lie in the lowermost part of the kyanite stability field, close to and partly overlapping with the kyanite/sillimanite join. As in the underlying Bozda© nappe, all calculations including ilmenite/rutile yielded unrealistically low pressures suggesting that ilmenite formed as a late retrograde phase.

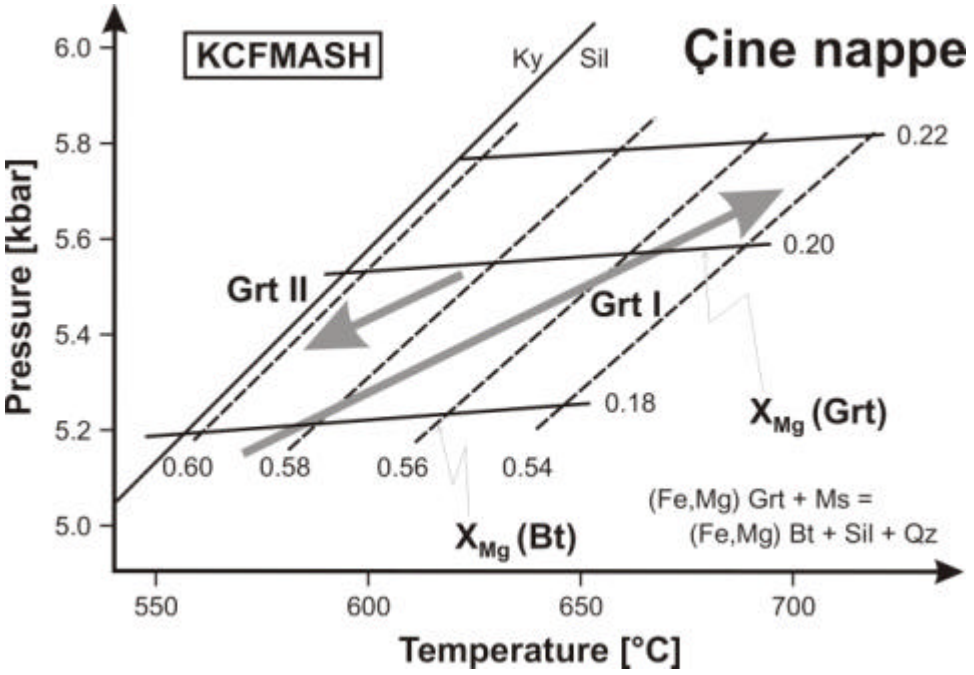

Fig. 8. Partial petrogenetic grid of reaction field of reaction (1) calculated for approximate compositional range of garnet and biotite in Çine metapelites in pure KCFMASH system. Activity of muscovite used is 0.8, while Al^{VI} in biotite is constantly set at 0.3 pfu and X_{Grs} in garnet at 0.03. Tentative paths during growth of grt I and II are indicated.

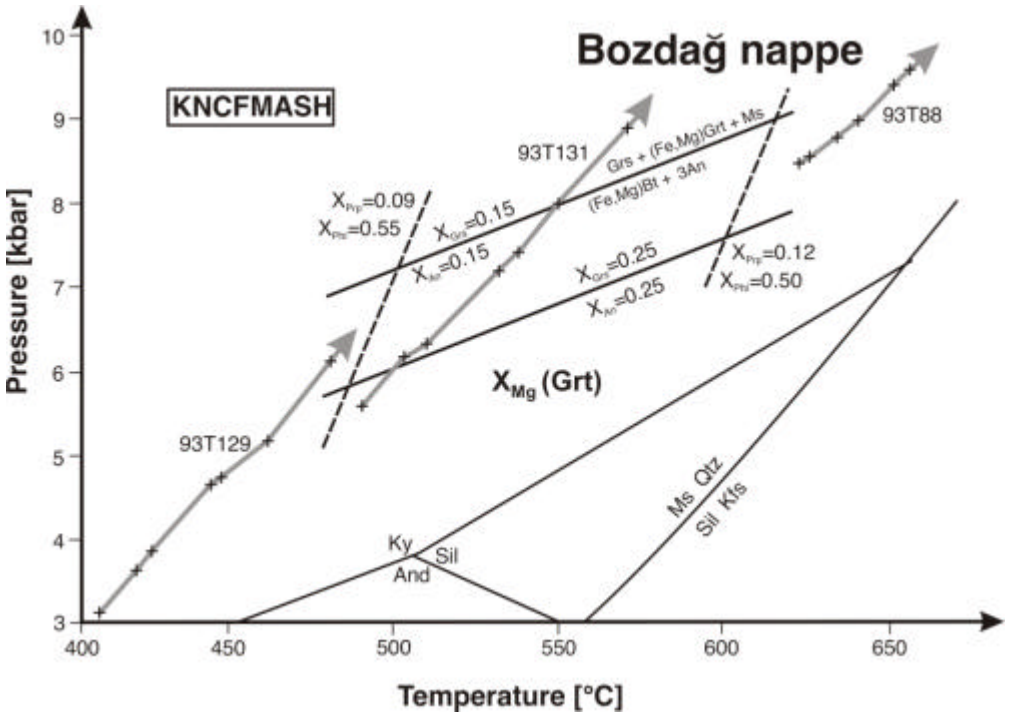

Fig. 9. Partial petrogenetic grid of reaction field of reaction (3) calculated for approximate compositional range of a typical Bozda© metapelite. Activity of muscovite is 0.8, Al^{VI} in biotite is constantly set at 0.3 pfu and X_{Grs} in garnet was set at 0.03. Prograde P-T path during growth of garnet as obtained from Gibbs modelling for garnet from samples 93T129, 93T131 and 93T88 (lower, middle and upper Bozda© nappe) are shown; crosses in modelled paths indicate successive calculation increments along a compositional profile.

Birgi metagranite.–The composition of garnet in the Birgi metagranite resembles grt II in the Çine metapelites with respect to composition and texture. Zoning is patchy and therefore geothermobarometry seems problematic. However, Si contents of 3.2 pfu of white mica in the limiting assemblage with biotite and K-feldspar indicate pressures of 6-7 kbar in the temperature range of 550-650?C according to the calibration of Massonne (1991). This would be in line with conditions during formation of grt II in the Çine metapelites.

Bozda© nappe

Peak P-T conditions for the metapelite of the Bozda© nappe were in the staurolite and partly also kyanite stability fields. In the lower (northern) part of the nappe, typical mineral assemblages of the staurolite+muscovite+quartz stability field are present (samples 93T129 and 93T148) (fig. 7). In the middle (sample 93T131) and upper (southern) part of the nappe (samples 93T50 and 93T88), the mineral assemblage represents the prograde staurolite+white mica+quartz breakdown curve:

staurolite + muscovite + quartz = biotite + garnet + kyanite + H_2O (5).

This is a prominent discontinuous reaction in the pure KFMASH system, which occurs at 650-700?C (Spear and Cheney, 1989). As the Bozda© metapelites have to be calculated as a KNCFMASH-system assemblage with additional Mn, the breakdown curve becomes continuous. Because of strong partitioning of Mn and Ca into garnet, the reaction curve can be expected to occur at considerably lower temperatures. This is consistent with preserved growth zoning in garnet. Increasing X_{Mg} from core to rim in the presence of biotite indicates prograde garnet growth. The significance of decreasing grossular content towards the rim in the presence of plagioclase for the relative sense of the

prograde P-T path is ambiguous as it depends on the compositional variation of plagioclase.

Differential thermodynamic modelling (Gibbs method) of garnet growth in the assemblage staurolite-quartz-muscovite-paragonite-biotite-H_20 (fig. 9) with starting conditions calculated from garnet rim and matrix-phase compositions (see below) shows: (1) A relatively steep prograde path during garnet growth. The paths for garnets from different structural levels of the Bozda© nappe are subparallel to each other. (2) The An content of plagioclase is higher during early garnet growth and decreases with progressive growth of garnet. (3) Modelling is impossible with additional kyanite in the above assemblage suggesting that kyanite was not in equilibrium with garnet during garnet growth and grew later.

Grossular is generally on the high-pressure side of multivariant garnet-forming reactions in Bozda© metapelite, such as reactions (2) and (3). In figure 9, reaction (3) and the Fe/Mg-exchange reaction between garnet and biotite was calculated and is shown for the approximate compositional variation of an average Bozda© metapelite. Variation of the muscovite activity has very little influence on the position of the garnet-forming reaction. Modelled P-T paths are consistent with the petrogenetic net (fig. 7). The slightly inverse Mn zonation at the outermost rims was probably induced by resorption of the outermost garnet rim due to breakdown of the grossular component of garnet during decompression at high temperature. This would result in a clockwise P-T path and would also explain increasing anorthite contents in the rims of plagioclase.

The restricted X_{Mg} variation in biotite is interpreted to be due to diffusion-controlled homogenization at the temperature peak, while the variation of Si and Al^{VI} reflects changing pressure and temperature conditions during biotite growth.

The two coexisting white micas indicate equilibration temperatures approximately between 450 and 600?C at 6-10 kbar according to the paragonite-muscovite solvus of Chatterjee and

Flux (1986). Such temperatures are in accord with the calculations of Ashworth and Evirgen (1985). Furthermore, paragonite is still stable in the presence of quartz. The maximum Si content of white mica in the paragenesis with kyanite, biotite and quartz is 3.15 pfu and would indicate a pressure of 8.5 kbar at 550?C (Massonne, 1991; pure MASH system). However, white mica with low Na content may also represent a second retrograde generation.

Maximum P-T conditions were calculated by combining garnet-rim compositions and adjacent biotite and white mica compositions (reaction (3) and garnet-biotite Fe/Mg-exchange reaction). As deduced from Gibbs modelling, plagioclase with the lowest anorthite contents is related with the garnet rims. Because garnet is resorbed, the calculated P-T conditions do not strictly represent peak metamorphic conditions. Temperature and pressure in the Bozda© nappe increases from 480-540?C/6.1-7.6 kbar at the base of the nappe to 560-580?C/8.5-8.9 kbar and to 610-660?C/8.5-10.8 kbar at the top of the nappe (table 2). Maximum temperatures might have been somewhat lower because no anatectic melts are observed. In samples 93T131 and 93T88, reaction (2) with coexisting kyanite yields maximum pressures that are 1-2 kbar higher than those of reaction (3) (table 2).

TECTONOMETAMORPHIC INTERPRETATION

P-T conditions in the Çine and Bozda© nappes and inferred P-T paths (figs. 8 and 9) are consistent with the petrogenetic calculations. For the lowermost Çine nappe, P-T conditions of 670-730?C/?6.2-6.3 kbar have been estimated and the P-T path appears to be anticlockwise. In the directly underlying Bozda© nappe, metamorphic conditions reached 610-660?C/8.5-10.8 kbar and differential thermodynamic modelling constrained the prograde P-T path during garnet growth. The P-T path in metapelite of the Bozda© nappe appears to be clockwise. Maximum P-T conditions were accomplished during the regional D_{PA} event, which occurred at ?540-550 Ma (Gessner et al., 2000a). Metamorphic rocks of both

nappes formed under different geothermal gradients and their P-T paths are apparently different from each other. Therefore, the Çine and Bozda© nappes cannot be regarded to belong to a tectonometamorphically homogeneous Pan-African basement as has been suggested by Candan and Dora (1997) and Candan et al. (2000).

P-T conditions in the Bozda© nappe are inverted and decrease structurally downward by ?40?C/?1 kbar per 1 km of structural section. Final emplacement of the Çine nappe directly above the Bozda© nappe and the inverted metamorphic field gradient in the Bozda© nappe should have occurred considerably after maximum P-T conditions were reached.

Another important conclusion of our work is that there is no evidence for an Alpine high-pressure overprint following the Pan-African amphibolite-facies metamorphism in the studied samples from both nappes. Ring et al. (1999b) and Gessner et al. (2000b) proposed that D_{A3} out-of-sequence thrusting of the middle tectonometamorphic unit, which correlates with the Cycladic blueschist unit and experienced Alpine high-pressure metamorphism, onto the Menderes nappes in the Eocene occurred after considerable exhumation (?35 km) of the middle tectonometamorphic unit and did therefore not cause Alpine high-pressure metamorphism in the Menderes nappes.

There are three general questions, which we address here: (1) What is the relationship between amphibolite-facies metamorphism, D_{PA} structures and emplacement of the eclogitic lenses? (2) How do the different P-T paths in the Çine and Bozda© nappes relate to the mechanism of juxtaposition of both nappes? (3) What may have caused the inverted metamorphic field gradient in the Bozda© nappe?

Amphibolite-facies metamorphism, D_{PA} structures and the eclogitic rocks

Microstructural relationships in the Çine and Bozda© nappes show that the formation of S_{PA} and growth of garnet (grt I in the

Çine nappe) occurred during increasing P-T conditions. Because the structures formed during prograde metamorphism, they most probably result from crustal shortening and thickening. There is no evidence for an earlier high-pressure metamorphism in the studied metapelite in either of the nappes. In the eclogitic rocks, D_{PA} occurred during decompression. Because the amphibolite-facies metamorphism of the eclogitic rocks occurred at 580-700?C/5-9.5 kbar (Candan and others, 2000), it seems that the amphibolite-facies overprint affected the eclogite, eclogitic gabbro and the surrounding metapelite and orthogneiss in both nappes at similar conditions. If this is accepted, it follows that the eclogitic rocks in the Çine and Bozda© nappes were sliced into both nappes during the contractional D_{PA} event after exhumation. The amount of eclogite exhumation was up to 30 km in the Çine nappe, whereas the exhumation of eclogitic gabbro in the Bozda© nappe was small (0-?15 km).

Different P-T paths in the Çine and Bozda© nappes

Peak-metamorphic temperatures in the upper Bozda© nappe are ?60?C lower but pressures are ?2-5 kbar higher than in the overlying Çine nappe and the shape of the P-T path of both nappes appears to be different. Prograde metamorphic conditions in the Bozda© nappe suggest a geothermal gradient of ?20?C km^{-1}. A higher gradient of ?30?C km^{-1} associated with widespread intrusion of granitoids at ?540-560 Ma is suggested for the Çine nappe. Isotopic work by Dannat (1997) revealed that the most probable tectonic setting for the Çine-nappe granitoids is a magmatic arc or a continent-collision zone. We discuss these two possible settings in which metamorphism and the juxtaposition of both nappes may have taken place.

Magmatic-arc setting.-The magmatic-arc option would be compatible with the relatively high field gradient in the Çine nappe and would suggest that granitoid intrusions and eclogite-facies metamorphism were in part coeval (fig. 10A). The field

gradient in the Bozda© nappe might be explained by nappe stacking during relatively cold conditions above the subduction zone (fig. 10B). The lack of ?540-560 Ma granitoids in the Bozda© nappe would be compatible with this tectonic position. Geometric constraints demand considerable displacement of the eclogite (but not necessarily of the eclogitic gabbro) during decompression (fig. 10).

Continent-collision setting.-A geothermal gradient of ?30?C km^{-1} has also been reported from collision belts like, for instance, the Lepontine dome of the Central Alps (see summary in Merle and Guillier, 1989). There, prograde amphibolite-facies metamorphism occurred during crustal imbrication of the lower Pennine nappes (which have no Alpine high-pressure overprint) following eclogite-facies metamorphism and exhumation in overlying nappes (e.g., Merle and Guillier, 1989; Ring, 1992; Schmid et al., 1996). Therefore, an alternative model to explain the different geothermal gradient in the Çine and Bozda© nappes may envision continent collision following eclogite-facies metamorphism (fig. 11). The implied drastic change in the thermal structure of the orogen would cause melting and the intrusion of widespread granitoids in the Çine nappe. In this case, eclogite-facies metamorphism would have to be older than the granitoids. The higher geothermal gradient in the Çine nappe would require a local upward deflection of isotherms within the developing orogen (fig. 11). This scenario would resemble in some respect the Tertiary evolution of the Lepontine dome in the Central Alps.

Discussion of tectonic settings.-Neither our thermobarometric data, nor the isotopic data of Dannat (1997) allow us to distinguish between the magmatic-arc and a continent-collision setting. Both options are not mutually exclusive because the granitoids may have evolved from arc granites to collision granites, i.e., that the subduction stage was followed by continent collision and both stages were accompanied by intrusion of granitic rocks.

The different P-T paths recorded in metapelite from the Çine and Bozda© nappes suggest that both nappes originated in different parts of the developing Pan-African orogen in western Turkey. This conclusion is further substantiated by late- to mainly postkinematic growth of grt II in the Çine nappe with respect to S_{PA} following peak-metamorphic conditions and the lack of this additional metamorphic event in the Bozda© nappe. Garnet II in the Çine nappe either grew during pressure increase following cooling or during near-isobaric cooling suggesting an overall anticlockwise P-T path. An anticlockwise

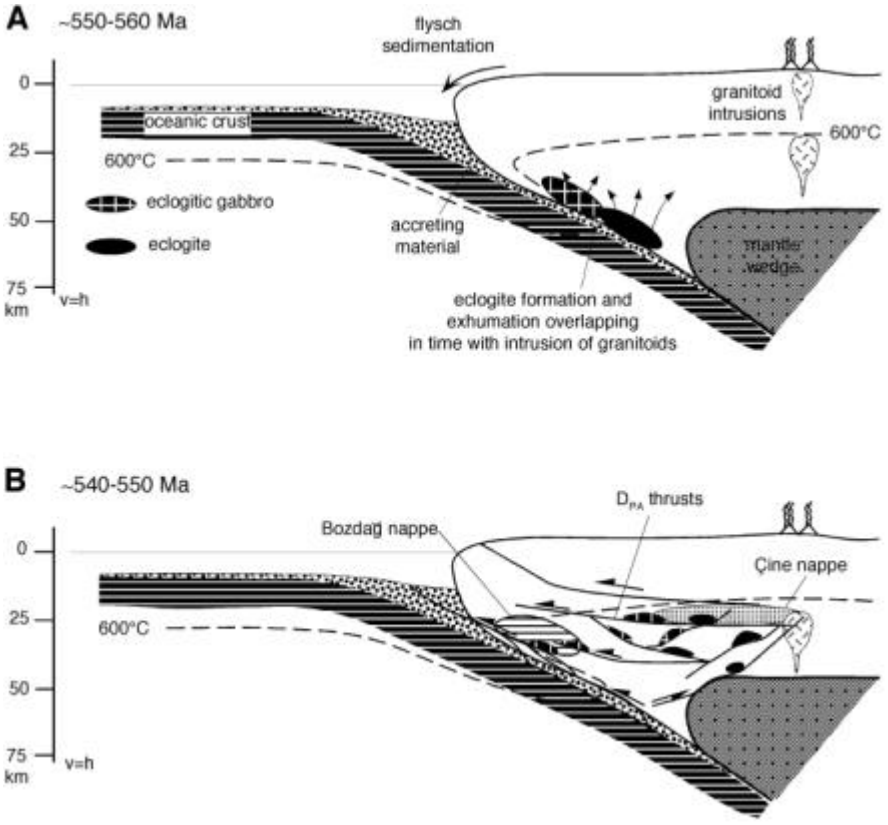

Fig. 10. Intrusion of Çine-nappe granitoids in magmatic-arc setting and amphibolite-facies metamorphism; 600?C isotherm is shown for reference. (A) Subduction, eclogite-facies metamorphism and flysch sedimentation in forearc and granitoid intrusions in magmatic arc. (B) Continued subduction, granitoid intrusions and D_{PA} thrusts; if arc-trench gap of 150 km and 30?-dipping subduction zone was assumed, displacement of eclogite on the order of >50 km would be indicated. The common occurrence of eclogite in Çine and Bozda© nappes suggests that these units came into proximity during D_{PA}, whereas very few <?540-Ma granitoids in Çine nappe and lack of these granitoids in Bozda© nappe may suggest that both nappes were not in close proximity at ?540-550 Ma. Note that the Çine nappe must have remained fairly stationary relative to the magmatic arc as indicated by intrusions from 540-560 Ma in Çine nappe.

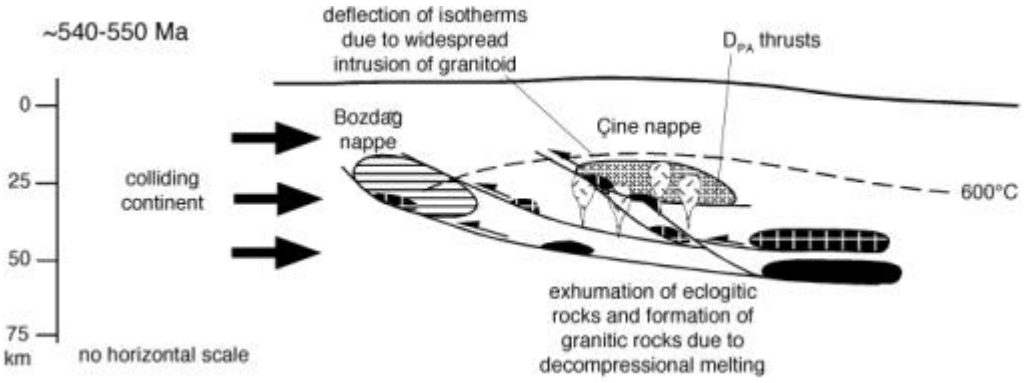

Fig. 11. Continent collision, amphibolite-facies metamorphism and granitoid intrusions following eclogite-facies metamorphism. A deflection of isotherms, probably caused by heating due to granitoid intrusions, is needed to explain different geothermal gradients in Çine and Bozda© nappes. Note that granitoids are deformed by D_{PA} thrusts but also crosscut them; position of Bozda© nappe relative to Çine nappe is unconstrained.

P-T path would suggest that the Çine nappe was sandwiched between two cooler units (cf. fig. 1C). A possible tectonic scenario would be widespread intrusion of granitoids and metamorphism in the Çine nappe followed and in part accompanied by emplacement of the latter onto a colder foreland unit. Emplacement of the hot Çine nappe caused burial, heating and a clockwise P-T path in this foreland unit. Kohn and others (1992) reported a similar case from the Appalachians, where rocks in the lower plate of a large thrust are characterized by a clockwise P-T path and rocks in the upper plate show isothermal loading followed by possible isobaric cooling. The P-T evolution of the Bozda© nappe leads us to speculate that it was part the foreland unit onto which the hot Çine nappe was emplaced at ?540-550 Ma. The difference in Pan-African peak pressure of ?2-5 kbar indicates that ?7-19 km of crust was between the lower Çine nappe and the upper Bozda© nappe.

Eocene juxtaposition of the Çine and Bozda© nappes.-The greenschist-facies top-to-the-S kinematic indicators at the nappe contact fit into a regionally consistent kinematic pattern of Eocene D_{A3} out-of-sequence thrusts, which assembled the Anatolide belt in western Turkey (Gessner et al., 2000b). Eocene movement at the Çine thrust, and also at the structurally deeper Bozda© thrust, cut the amphibolite-facies isograds at an acute angle (fig. 4). The albite porphyroclasts show a strong spatial association with the Alpine nappe boundaries, especially at the contact of the Bozda© nappe with the underlying Bayindir nappe and grew during a static growth event after Alpine nappe emplacement. The up to 19 km thick crustal section, which is missing between the Çine and Bozda© nappes, may have been excised during D_{A3} out-of-sequence thrusting.

Inverted metamorphism in the Bozda© nappe

The inverted thermal field gradient in the Bozda© nappe has already been reported by Izdar (1971) and Hetzel (1995). Ashworth and Evirgen (1985) showed that the inverted thermal field gradient is accompanied by an inverted pressure gradient. Hetzel (1995) and Hetzel et al. (1998) compared the inverted thermal field gradient with that of the Higher Himalayan Crystalline sequence above the Main Central thrust. In some parts of the Higher Himalayan Crystalline sequence, an inverted temperature field gradient has been detected above the Main Central thrust (e.g., Mallet, 1875; Hubbard, 1989), whereas in other parts, thermometry revealed only limited temperature variations around ?600?C (e.g., Metcalfe, 1993). Vannay and Grasemann (1998) showed that this apparent lack of a temperature field gradient is a consequence of re-equilibration of the widely used garnet-biotite thermometer during cooling. Vannay et al. (1999) used phase equilibria, oxygen-isotope thermometry and barometry to show that there is an upward temperature increase from ?570?C to ?750?C. However, because this inverted thermal field gradient occurred at a constant pressure of ?8 kbar it is different from the inverted metamorphic field gradient in the Bozda© nappe.

The five samples analyzed by us do not allow us to distinguish whether or not the inverted field gradient in the Bozda© is a continuous feature across the whole nappe without breaks (fig. 12A), or is a discontinuous feature caused by a series of within-nappe imbrications (fig. 12B). The metamorphic facies maps of Izdar (1971) and Ashworth and Evirgen (1985) may suggest that it is a continuous feature and a simple explanation would be that the whole Bozda© nappe was turned upside down
during the Alpine orogeny, i.e. the Bozda© nappe represents the lower limb of a recumbent fold (fig. 12A) and the upper limb of this fold has been sheared out. Okay (2000) has recently proposed that the whole Anatolide orogen of western Turkey is a gigantic recumbent fold on the 100-km scale. Although the inverted

metamorphic field gradient in the studied part of the Bozda© nappe only demands recumbent folding on the <10 km scale, we are reluctant to propose such a fold (see discussion in Gessner and others, 2000c). Large-scale folding in the central Ödemi{ submassif (fig. 3) occurred during rotation of the bivergent detachment system after the Late Miocene (Gessner, 2000) and no solid field evidence for other large-scale folds has been reported from the Anatolide belt in western Turkey so far. The deformation history recently proposed by Gessner et al. (2000b) shows no evidence for Alpine recumbent folding in the Bozda© nappe, which preceded the emplacement of the Çine nappe above the Bozda© nappe.

We interpret that the currently available data to suggest that the inverted metamorphic field gradient is a non-continuous feature caused by a few (2-3) Alpine top-to-the-S displacing thrusts in the Bozda© nappe (fig. 12B). Hetzel (1995) mapped greenschist-facies top-to-the-S shear zones in the Bozda© nappe, but further detailed field work is needed to demonstrate that these shear zones can explain the inverted metamorphic field gradient in the Bozda© nappe.

CLOSING REMARKS

An amphibolite-facies metamorphic event affected the Çine and Bozda© nappes of the Anatolide orogen of western Turkey during the Pan-African orogeny. Peak-metamorphic conditions in the lowermost Çine nappe are 670-730?C/?6.2-6.3 kbar. Prograde garnet growth (grt I) occurred during the D_{PA} event. Formation of a second, discordantly overgrowing garnet generation followed at 550-620?C/?6.4-6.5 kbar, probably during near-isobaric cooling. Peak-metamorphic conditions in the underlying Bozda© nappe vary from 480-540?C/6.1-7.6 kbar at the base to 610-660?C/8.5-10.8 kbar at the top of the nappe and attest to an inverted metamorphic field gradient. The P-T paths in both nappes are different from one another and reflect metamorphism in different parts of the evolving Pan-African orogen in western Turkey, i.e.,

D_{PA} affected different tectonometamorphic units in different orogenic positions during crustal shortening. Although the D_{PA} event did not directly juxtapose the Çine nappe with the Bozda© nappe, we believe that the P-T path of metapelite in the Bozda© nappe was in part controlled by emplacement of the hot Çine nappe. Amphibolite-facies metamorphism and widespread granitoid intrusions in the Çine nappe either occurred in a magmatic-arc or a continent-collision setting.

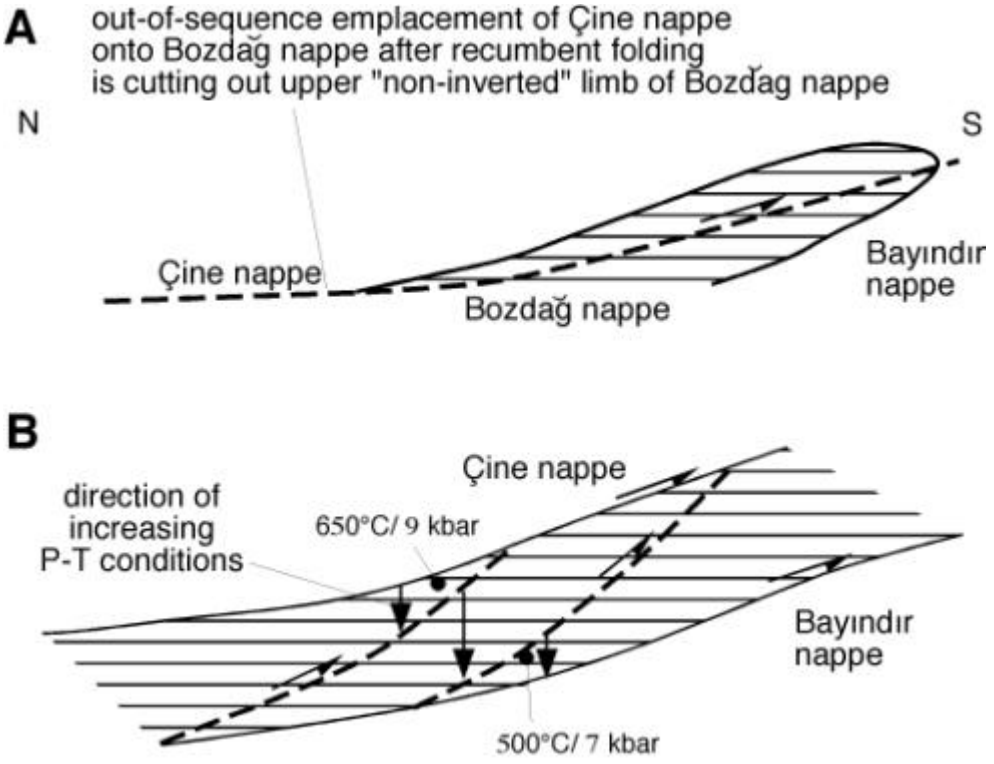

Fig. 12. (A) Inverted metamorphic field gradient in Bozda© nappe interpreted to be continuous feature caused by Alpine recumbent folding and subsequent D_{A3} thrusting of Çine nappe onto Bozda© nappe. (B) Inverted metamorphic field gradient interpreted to result from Alpine imbrication within Bozda© nappe, which placed higher-grade Pan-African metamorphics above lower-grade ones.

Both options can be tested by constraining the age of eclogite-facies metamorphism in the eclogitic lenses in both nappes.

The inverted metamorphic field gradient in the Bozda© nappe was probably caused during Alpine nappe stacking. The inversion may have been caused by large-scale recumbent folding or, as we prefer, by internal imbrication. Both options can be tested by further tectonometamorphic field studies.

ACKNOWLEDGEMENTS

Funded by the Deutsche Forschungsgemeinschaft (grants Ri 538/4-1, 4-2 and 4-3). Reviews by Dov Avigad, Andreas Möller, Aral Okay and especially Donna Whitney were helpful. Ralf Hetzel provided the samples analyzed in this study. We thank Thomas Reinecke for help with the Gibbs method and Klaus Gessner for a pre-submission review and drawing of Figs. 2-4. UR likes to thank Alfred Kröner

for his continuous support, encouragement and friendship since 1992.

References

Ashworth, J.R., Evirgen, M.M., 1985, Plagioclase relations in pelites, central Menderes Massif, Turkey. I: The peristerite gap with coexisitng kyanite: Journal of Metamorphic Geology, p. 3, p. 207-218.

Berman, R.G., 1988, Internally-consistent thermodynamic data for minerals in the system Na_2O-K_2O-CaO-MgO-FeO-Fe_2O_3-Al_2O_3-SiO_2-TiO_2-H_2O-CO_2: Journal of Petrology, v. 29, p. 445-522.

Berman, R.G.,1990, Mixing properties of Ca-Mg-Fe-Mn garnets: American Mineralogist, v. 75, p. 328-344.

Bertrand, M., 1884, Rapport de structure des Alpes de Glaris et du bassin houiller du Nord. Bulletin Geologie de France 3, v. 12, p. 318-330.

Bozkurt, E., Park, R.G., Winchester, J.A., 1993, Evidence against the core/cover interpretation of the southern sector of the Menderes Massif, west Turkey: Terra Nova, v. 5, p. 445-451.

Brown, T.H., Berman, R.G., Perkins, E.H., 1989, Ge0-Calc: Software package for calculation and display of pressure-temperature-composition phase diagrams using an IBM or compatible Personal Computer: Computer and Geoscience, v. 14, p. 279-289.

Ça©layan, M.A., Ötztürk, E.M., Ötztürk, S., Sav, H., Akat, U., 1980, Menderes Masifi güneyine ait bulgular ve yapisal yorum: Geological Engineering, v. 10, p. 9-19.

Candan, O., Dora, Ö.O., 1997, Generalized geological map of the Menderes Massif: Dokuz Eylül University, Bornova, Turkey.

Candan, O., Dora, Ö.O., Oberhänsli, R., Çetinkaplan, M., Partzsch, J.H., Warkus, F.C., Dürr, S., 2000, Pan-African high-pressure metamorphism in the Precambrian basement of the Menderes Massif, western Anatolia, Turkey. Geologische Rundschau, v. 89, in press.

Candan, O., Dora, Ö.O., Oberhänsli, R., Oelsner, F., Dürr, S., 1997, Blueschist relics in the Mesozoic cover series of the Menderes Massif and correlations with Samos Island, Cyclades. Schweizerische Mineralogische und Petrographische Mitteilungen, v. 77, p. 95-99.

Chatterjee, N.D., Flux, S., 1986, Thermodynamic mixing properties of muscovite-paragonite crystalline solutions at high temperatures and pressures, and their geological applications: Journal of Petrology, v. 27, p. 677-693.

Chatterjee, N.D., Froese, F., 1975, A thermodynamic study of the binary join muscovite-paragonite in the system $KalSi_3O_8$-$NaAlSi_3O_8$-Al_2O_3-SiO_2-H_2O: American Mineralogist, v. 60, p. 985-993.

Dannat, C., 1997, Geochemie, Geochronologie und Nd- und Sr-Isotopie der granitoiden Kerngneise des Menderes Massivs, SW-Türkei: Unpublished Ph.D. thesis, Universität Mainz, 120p.

Dannat, C., Reischmann, T., 1999, Single zircon ages of migmatites from the Menderes Massif, SW Turkey: Journal of Conference Abstracts, v. 4, p. 805.

Engel, M., Reischmann, T., 1998, Single zircon geochronology of orthogneisses from Paros, Greece: Bulletin of the Geological Society of Greece, v. 32, p. 91-99.

England, P. C., Richardson, S. W., 1977, The influence of erosion upon the mineral facies of rock from different metamorphic environments: Journal Geological Society of London, v. 134, p. 201-213.

England, P.C., Thompson, A.B., 1984, Pressure-temperature-time paths of regional metamorphism I. Heat transfer during the evolution of thickened continental crust: Journal of Petrology, v. 24, p. 894-928.

Fuhrman, M.L., Lindsley, D.H., 1988, Ternary-feldspar modeling and thermometry: American Mineralogist, v. 73, p. 201-216.

Gessner, K., Piazolo, S., Güngör, T., Ring, U., Kröner, A., Passchier, C.W., 2000a, Tectonic significance of deformation patterns in granitoid rocks of the Menderes nappes, Anatolide belt, southwest Turkey: Geologische Rundschau, v. 89, in press.

Gessner, K., Ring, U., Passchier, C.W., Güngör, T., 2000b, The Cyclades in Turkey: Evidence for Eocene post-high-pressure emplacement of the Cycladic blueschist unit onto the Menderes nappes, Anatolide belt, western Turkey: Tectonics, submitted.

Gessner, K., Ring, U., Hetzel, R., Passchier, C.W., 2000c, Stratigraphic and metamorphic inversions in the central Menderes Massif: a new structural model: comment: Geologische Rundschau, submitted.

Hetzel, R., 1995, The Alpine tectono-metamorphic evolution of the central Menderes Massif, southwestern Turkey: Unpublished Ph.D. thesis, Universität Mainz, 78p.

Hetzel, R., Ring, U. Akal, C., Troesch, M., 1995a, Miocene NNE-directed extensional unroofing in the Menderes Massif, southwestern Turkey: Journal of the Geological Society of London, v. 152, p. 639-654.

Hetzel, R., Passchier, C.W., Ring, U., Dora, Ö.O., 1995b, Bivergent extension in orogens: The Menderes Massif (southwestern Turkey): Geology, 23, 455-458.

Hetzel, R., Reischmann, T., 1996, Intrusion age of Pan-African augen gneiss in the southern Menderes Massif and the age of cooling after Alpine ductile extensional deformation: Geological Magazine, v. 133, p. 565-572.

Hetzel, R., Romer, R.L., Candan, O., Passchier, C.W., 1998, Geology of the Bozdag area, central Menderes Massif, SW Turkey: Pan-African basement and Alpine deformation. Geologische Rundschau, v. 87, p. 394-406.

Holdaway, M.J., 1971, Stability of andalusite and the aluminium phase diagram: American Journal of Science, v. 271, p. 97-131.

Hubbard, M.S., 1989, Thermobarometric constraints on the thermal history of the Main Central Thrust Zone and Tibetan slab, eastern Nepal Himalaya. Journal of Metamorphic Geology, v. 7, p. 19-30.

Isik, V., Tekeli, O., 2000, Late orogenic crustal extension in northern Menderes Massif (western Turkey): evidence for metamorphic core complex formation: Geologische Rundschau, v. 89, in press.

Izdar, E., 1971, Introduction to the geology and metamorphism of the Menderes Massif of western Turkey. In: Campell, A.S. (ed), Geology and history of Turkey, p. 495-500.

Johannes, W., 1985, Beginning of melting in the granite system Qz-Or-Ab-An-H_2O: Contributions to Mineralogy and Petrology, v. 86, p. 264-273.

Kohn, M.J., Orange, D.L., Spear, F.S., Ruble, D., Harrison, T.M., 1992, Pressure, temperature, and structural evolution of west-central New Hampshire: Hot thrust over cold basement: Journal of Petrology, v. 33, p. 521-556.

Koralay, E., Satir, M., Dora, O., 2000, Geochemical and geochronological evidence for Early Triassic calc-alkaline magmatism in the Menderes Massif, western Turkey: Geologische Rundschau, v. 89, in press.

Kröner, A., „engör, A.M.C., 1990, Archean and Proterozoic ancestry in late Precambrian to early Paleozoic crustal elements of southern Turkey as revealed by single-zircon dating: Geology, v. 18, p. 1186-1190.

Lackmann, W., 1997, P-T Entwicklung von Metapeliten des zentralen Menderes Massiv, Türkei: Unpublished Diploma thesis, Universität Mainz, 106p.

Lapworth, C. 1883. On the secret of the Highlands. Geological Magazine, 10, 120-128 and 193-199.

Lugeon, M. 1901. Les grande nappes de récouvrement des Alpes du Chablais et de la Suisse. Bulletin de la Société Géologique de France, 4^{th} series, 1, 723-825.

Lips, A.L.W., 1998, Temporal constraints on the kinematics of destabilization of an orogen: syn- to post-orogenic collapse of the Northern Aegean region: Geologicae Ultraiectae, v. 166, p. 1-223.

Loos, S., Reischmann, T., 1999, The evolution of the southern Menderes Massif in SW Turkey as revealed by zircon dating: Journal of the Geological Society of London, v. 156, p. 1021-1030.

Mallet, F.R., 1875, On the geology and mineral ressources of the Darjiling district and the western Duars. Memoir Geological Survey of India, v. 11, p. 1-50.

Massonne, H.-J., 1991, High pressure, low-temperature metamorphism of pelitic and other protoliths based on experiments in the system K_2O-MgO-Al_2O_3-SiO_2-H_2O: Unpublished Habiltation thesis, Universität Bochum, Germany, 172 p.

McMullin, D.W., Berman, R.G., Greenwood, H.J., 1991, Calibration of the SGAM thermometer for pelitic rocks using data from equilibrium experiments and natural assemblages: Canadian Mineralogist, v. 29, p. 889-908.

Merle, O., Guillier, B., 1989, The building of the Swiss Alps: an experimental approach: Tectonophysics, v. 165, p. 41-56.

Metcalfe, R.P., 1993, Pressure, temperature and time constraints on metamorphism across the Main Central Thrust zone and High Himalayan Slab in the Garhwal Himalaya. In: Treloar, P.J., Searle, M.P. (eds) Himalayan tectonics. Special Publications of the Geological Society of London, v. 74, p. 485-509.

Oberhänsli, R., Candan, O. Dora, O.Ö., Dürr, H.S., 1997, Eclogites within the Menderes crystalline complex, western Turkey, Anatolia: Lithos, v. 41, p. 135-150.

Okay, A.I., 2000, Stratigraphic and metamorphic inversion in the central Menderes Massif: a new structural model: Geologische Rundschau, v. 89, in press.

Reinecke, T., 1998, Prograde high- to ultrahigh-pressure metamorphism and exhumation of oceanic sediments at Lago di Cignana, Zermatt-Saas Zone, western Alps: Lithos, v. 42, p. 147-189.

Reischmann, T., 1997, Single zircon Pb/Pb dating of tectonic units from the metamorphic complex of Naxos, Greece. Terra abstracts, v. 9, p. 496.

Reischmann, T., 1998, Pre-Alpine origin of tectonic units from the metamorphic complex of Naxos, Greece, identified by single zircon Pb/Pb dating: Bulletin of the Geological Society of Greece, v. 32, p. 101-111.

Ring, U., 1992: The Alpine geodynamic evolution of Penninic nappes in the eastern Central Alps: geothermobarometric and kinematic data: Journal of Metamorphic Geology, v. 10, p. 33-53.

Ring, U., Laws, S., Bernet, M., 1999a, Structural analysis of a complex nappe sequence and late-orogenic basins from the Aegean Island of Samos, Greece: Journal of Structural Geology, v. 21, p. 1575-1601.

Ring, U., Gessner, K., Passchier, C.W., Güngör, T., 1999b, The Menderes Massif of western Turkey and the Cycladic Massif in the Aegean – do they really correlate: Journal of Geological Society of London, v. 156, p. 3-6.

Schmid, S.M., Pfiffner, O.A., Froitzheim, N., Schönborn. G., Kissling, E., 1996, Geophysical-geological transect and tectonic evolution of the Swiss-Italian Alps: Tectonics, v. 15, p. 1036-1064.

Schuiling, R.D., 1962, On petrology, age, and structure of the Menderes migmatite complex (SW-Turkey): Bulletin of the Mineral Resources and Exploration Institute of Turkey, v. 58, p. 71-84.

„engör, A.M.C, 1987, Cross faults and differential stretching in their hanging walls in regions of low-angle normal faulting: examples from western Turkey. In: Coward, M.J., Dewey, J.F., Hancock, P.L. (eds) Continental extensional

tectonics. Special Publications of the Geological Society of London, v. 28, p. 405-473.

„engör, A.M.C., Satir, M., Akkök, R., 1984, Timing of tectonic events in the Menderes Massif, western Turkey: Implications for tectonic evolution and evidence for Pan-African basement in Turkey: Tectonics, v. 3, p. 693-707.

Spear, F.S., Cheney, J.T., 1989, A petrogenetic grid for pelitic schists in the system SiO_2-Al_2O_3-Fe_2O_3-MgO-K_2O-H_2O: Contributions to Mineralogy and Petrology, v. 101, p. 149-164.

Spear, F.S., Peacock, S.M., Kohn, M.J., Florence, F.P., Menard, T., 1991. Computer programs for petrologic P-T-t path calculations: American Mineralogist, v. 76, p. 2009-2012.

Termier, P., 1899. Les nappe de récouvrement du Briançonnais. Bulletin de la Société Géologique de France, 3rd series, 27, 47-84.

van der Linth, A.E., 1846, Gebirgskunde: Historisch-geographisch-statistische Gemälde der Schweiz, v.7, pp.51.

Vannay, J.C., Grasemann, B., 1998, Inverted metamorphism in the High Himalaya of Himachal Pradesh (NW India): phase equilibria versus thermobarometry: Schweizerische Mineralogische und Petrographische Mitteilungen, v. 78, p. 109-135.

Vannay, J.C., Sharp, Z.D., Grasemann, B., 1999, Himalayan inverted metamorphism constrained by oxygen isotope thermometry: Contributions to Mineralogy and Petrology, v. 137, p. 90-101.

Whitney, D.L., Dilek, Y., 1998, Metamorphism during crustal thickening and extension in central Anatolia: the Nigde metamorphic core complex: Journal of Petrology, v. 9, p. 1385 – 1403.

Willner, A.P., 1992, "Fibrolithisierung", ein Fluid-Gesteins-Interaktionsphänomen auf dem prograden P-T-Pfad: European Journal of Mineralogy, v. 4, p. 295.

Willner, A.P., 1995, Pressure-temperature evolution of a low-pressure amphibolite facies terrane in Central Bushmanland (Namaqua Mobile Belt; South Africa): Special Publication Communications of the Geological Survey of Namibia, v. 15, p. 5-19.